AGU PUBLICATIONS

JGR

Journal of Geophysical Research: Oceans

RESEARCH ARTICLE

10.1002/2017JC013279

Key Points:

- Contribution of nonalgal particles to particulate absorption is large ($23 \pm 17\%$) and no relationship observed between them and chlorophyll *a*
- Phytoplankton-specific absorption is higher, for a given chlorophyll *a* concentration, than those derived from global relationships
- Variations in phytoplankton-specific absorption are observed due to changes in phytoplankton size as well as in photoprotective pigments

Correspondence to:
M. Kheireddine,
malika.kheireddine@kaust.edu.sa

Citation:
Kheireddine, M., Ouhssain, M., Organelli, E., Bricaud, A., & Jones, B. H. (2018). Light absorption by suspended particles in the Red Sea: Effect of phytoplankton community size structure and pigment composition. *Journal of Geophysical Research: Oceans*, *123*, 902–921. https://doi.org/10.1002/2017JC013279

Received 16 JUL 2017
Accepted 3 JAN 2018
Accepted article online 9 JAN 2018
Published online 3 FEB 2018

Light Absorption by Suspended Particles in the Red Sea: Effect of Phytoplankton Community Size Structure and Pigment Composition

Malika Kheireddine[1], Mustapha Ouhssain[1,2,3], Emanuele Organelli[4], Annick Bricaud[2,3], and Burton H. Jones[1]

[1]Biological and Environmental Sciences and Engineering Division, Red Sea Research Center, King Abdullah University of Science and Technology, Thuwal, Saudi Arabia, [2]Sorbonne Universités, UPMC Univ Paris 06, UMR 7093, LOV, Observatoire Océanologique, Villefranche-Sur-Mer, France, [3]CNRS, UMR 7093, LOV, Observatoire Océanologique, Villefranche-Sur-Mer, France, [4]Plymouth Marine Laboratory, Plymouth, UK

Abstract The light absorption properties of phytoplankton ($a_{ph}(\lambda)$) and nonalgal particles ($a_{nap}(\lambda)$) associated with phytoplankton pigments were analyzed across the Red Sea, in the upper 200 m depth, between October 2014 and August 2016. The contribution by nonalgal particles to the total particulate light absorption ($a_{ph}(\lambda) + a_{nap}(\lambda)$) was highly variable ($23 \pm 17\%$ at 440 nm) and no relationship between $a_{nap}(440)$ and chlorophyll *a* concentration, [TChl *a*], was observed. Phytoplankton-specific phytoplankton absorption coefficients at 440 and 676 nm for a given [TChl *a*], a_{ph}*(440), and $a^*_{ph}(676)$ were slightly higher than those derived from average relationships for open ocean waters within the surface layer as well as along the water column. Variations in the concentration of photosynthetic and photoprotective pigments were noticeable by changes in phytoplankton community size structure as well as in $a^*_{ph}(\lambda)$. This study revealed that a higher proportion of picophytoplankton and an increase in photoprotective pigments (mainly driven by zeaxanthin) tended to be responsible for the higher $a^*_{ph}(\lambda)$ values found in the Red Sea as compared to other oligotrophic regions with similar [TChl *a*]. Understanding this variability across the Red Sea may help improve the accuracy of biogeochemical parameters, such as [TChl *a*], derived from in situ measurements and ocean color remote sensing at a regional scale.

1. Introduction

Light absorption coefficients by suspended particles, $a_p(\lambda)$, i.e., phytoplankton ($a_{ph}(\lambda)$) plus nonalgal particles ($a_{nap}(\lambda)$), are key parameters that determine the optical signature of oceanic waters and affect the color of the ocean. The natural variability of these coefficients in various oceanic regions has been studied to establish global bio-optical relationships. Based on these studies, algorithms for the retrieval of biogeochemical products (e.g., [TChl *a*]) from in situ or ocean color remote sensing have been refined (Atlas & Bannister, 1980; Garver & Siegel, 1997; Kiefer & Mitchell, 1983; Maritorena et al., 2002; Morel, 1991; Morel & Bricaud, 1981; Morel et al., 2006; Morel & Maritorena, 2001; Roesler & Perry, 1995; Sathyendranath et al., 2001). Furthermore, these coefficients, and the phytoplankton-specific phytoplankton absorption coefficient ($a_{ph}*(\lambda)$) in particular, are also relevant for primary production models and for inferring phytoplankton size and taxonomic composition (Bracher et al., 2017; Ciotti & Bricaud, 2006; Platt & Sathyendranath, 1988; Sathyendranath & Platt, 1988; Tilstone et al., 2014; Uitz et al., 2010). Indeed $a_{ph}*(\lambda)$ is, at the first order, driven by the concentration in phytoplankton biomass (Bricaud et al., 1998, 2010; Cleveland, 1995; Mitchell & Kiefer, 1988) and, at the second order, by phytoplankton size and taxonomic structure as well as pigment composition and proportions (Bricaud et al., 1995, 2004; Ciotti & Bricaud, 2006; Ciotti et al., 2002; Devred et al., 2006). Thus, understanding the variability of $a_{ph}*(\lambda)$ with respect to [TChl *a*], phytoplankton community structure and pigment composition is of primary relevance for biogeochemical studies and ocean color remote sensing applications (Morel & Bricaud, 1981; Roesler & Perry, 1995; Sathyendranath et al., 2001).

While the variations in $a_{ph}(\lambda)$ and $a_{nap}(\lambda)$ have been extensively studied in various area of the global ocean (Bricaud et al., 1995, 1998, 2010; Boss et al., 2013a; Devred et al., 2006; Lutz et al., 1996; Suzuki et al., 1998), few studies have been performed in the Red Sea (Brewin et al., 2015, Organelli et al., 2017) during the last three decades. Recently, Brewin et al. (2015) suggested that the Red Sea waters and their optical characteristics can be affected by its different hydrological, biological and environmental conditions (low precipitation, little riverine input, and desert dust events), giving rise to distinct bio-optical relationships in some subareas of this sea. Using field or ocean color remote sensing observations to infer biogeochemical parameters (e.g., $a_{ph}(\lambda)$, [TChl *a*]) from previously established bio-optical models, therefore, may introduce uncertainties in the retrieved products (Organelli et al., 2017). When analyzing the bio-optical characteristics of the Red Sea, Brewin et al. (2015) observed that the relationship established between the particulate backscattering coefficient and [TChl *a*] as well as the relationship between $a_p(\lambda)$ and [TChl *a*] were similar to those parameterized by Brewin et al. (2011) and Bricaud et al. (1998) for other clear waters, respectively. Thus, they suggested that the overestimation of remotely sensed [TChl *a*] concentrations in the Red Sea, as derived from standard bio-optical algorithms, could be due to an excess of colored dissolved organic matter (CDOM) absorption per unit of [TChl *a*]. However, Organelli et al. (2017) did not observe bio-optical anomalies in the Red Sea, when analyzing measurements of diffuse attenuation coefficient for downward irradiance at those wavelengths used as proxies of CDOM and phytoplankton light absorption coefficients (Morel et al., 2007). In these studies, measurements were only taken during a limited period of the year (fall-winter season), either restricted to the surface layer or in a given subregion of the Red Sea. It is now well known that changes in optical properties can depend on modifications of proportions between the optically significant substances (CDOM, nonalgal particles and phytoplankton) observed over seasons (Devred et al., 2006; Organelli et al., 2014; Sathyendranath et al., 1999). Therefore, further characterization of the bio-optical behavior of the Red Sea is required.

The Red Sea is one of the most saline and warmest deep seas in the world (Belkin, 2009; Longhurst, 2007; Raitsos et al., 2011, 2013) characterized by low precipitation, little riverine input (Patzert, 1974), and high evaporation rates (Sofianos & Johns, 2003). The Red Sea displays pronounced south-north latitudinal gradients in environmental conditions such as temperature, salinity, light intensity, and nutrients (Churchill et al., 2014; Ismael, 2015; Neumann & McGill, 1962; Raitsos et al., 2013; Sawall et al., 2014; Sofianos & Johns, 2003). The Red Sea is considered as a large marine ecosystem (Belkin, 2009) and sustains coral reefs, mangroves, and seagrass beds, which provide habitat for a large variety of marine organisms (Almahasheer et al., 2016; Berumen et al., 2013). The Red Sea is known as an oligotrophic basin given the depletion of nutrients in the surface layer (Racault et al., 2015; Raitsos et al., 2013, 2015; Triantafyllou et al., 2014).

Several studies showed that the seasonal variability of phytoplankton biomass in the Red Sea appears to be controlled by physical processes (winter mixing, mesoscale eddies, horizontal advection, and intrusion of water masses from Bab-el-Mandeb) that determine the availability of nutrients to the euphotic layer (Dreano et al., 2016; Gittings et al., 2017; Racault et al., 2015; Raitsos et al., 2013, 2015; Triantafyllou et al., 2014; Wafar et al., 2016). Recently, Pearman et al. (2016) and Kheireddine et al. (2017) showed that phytoplankton community structure (size and taxonomy) and its spatiovertical distribution appear to adapt in response to changes in environmental conditions along the south-north latitudinal gradients. They observed that picophytoplankton were generally the most abundant group at the surface along the whole basin. Nanophytoplankton, such as pelagophytes and prymnesiophytes, mainly characterized the community structure below the surface down to a depth of 150 m. In the Southern Red Sea, microphytoplankton (diatoms) were more prominent at the bottom of the euphotic layer. Pearman et al. (2016) suggested that this distribution correlated with increased nutrients found in this region, caused by the inflow of nutrient-rich water from the Gulf of Aden. How this variability in phytoplankton size structure, and thus in photosynthetic and photoprotective pigment concentrations, influences both $a_{ph}(\lambda)$ and $a^*_{ph}(\lambda)$ along the water column remains unknown.

A unique data set of high-performance liquid chromatography-derived phytoplankton pigments and spectral light absorption coefficients of phytoplankton and nonalgal particles has been compiled for the upper 200 m water column across the Red Sea basin. This data set will increase the understanding of the bio-optical properties of this region and, with a focus on surface waters, evaluate the feasibility to retrieve biogeochemical quantities with better accuracy from ocean color observations. In particular, this study aims to (1) examine the relationships linking $a_p(\lambda)$, $a_{ph}(\lambda)$, and $a_{nap}(\lambda)$ to phytoplankton biomass ([TChl *a*]), (2) assess the influences of phytoplankton cell size and pigment composition on the variability in light absorption properties, and (3) identify presence/lack of consistency between the bio-optical relationships established in Red Sea waters and those parameterized for other oceanic areas around the world.

2. Materials and Methods

2.1. Oceanographic Cruises and Sampling

Samples were collected during five research cruises performed across the Red Sea between October 2014 and January 2016 on board of the R/V Thuwal. Two cruises named as CRS-01, and CRS-04 took place in the

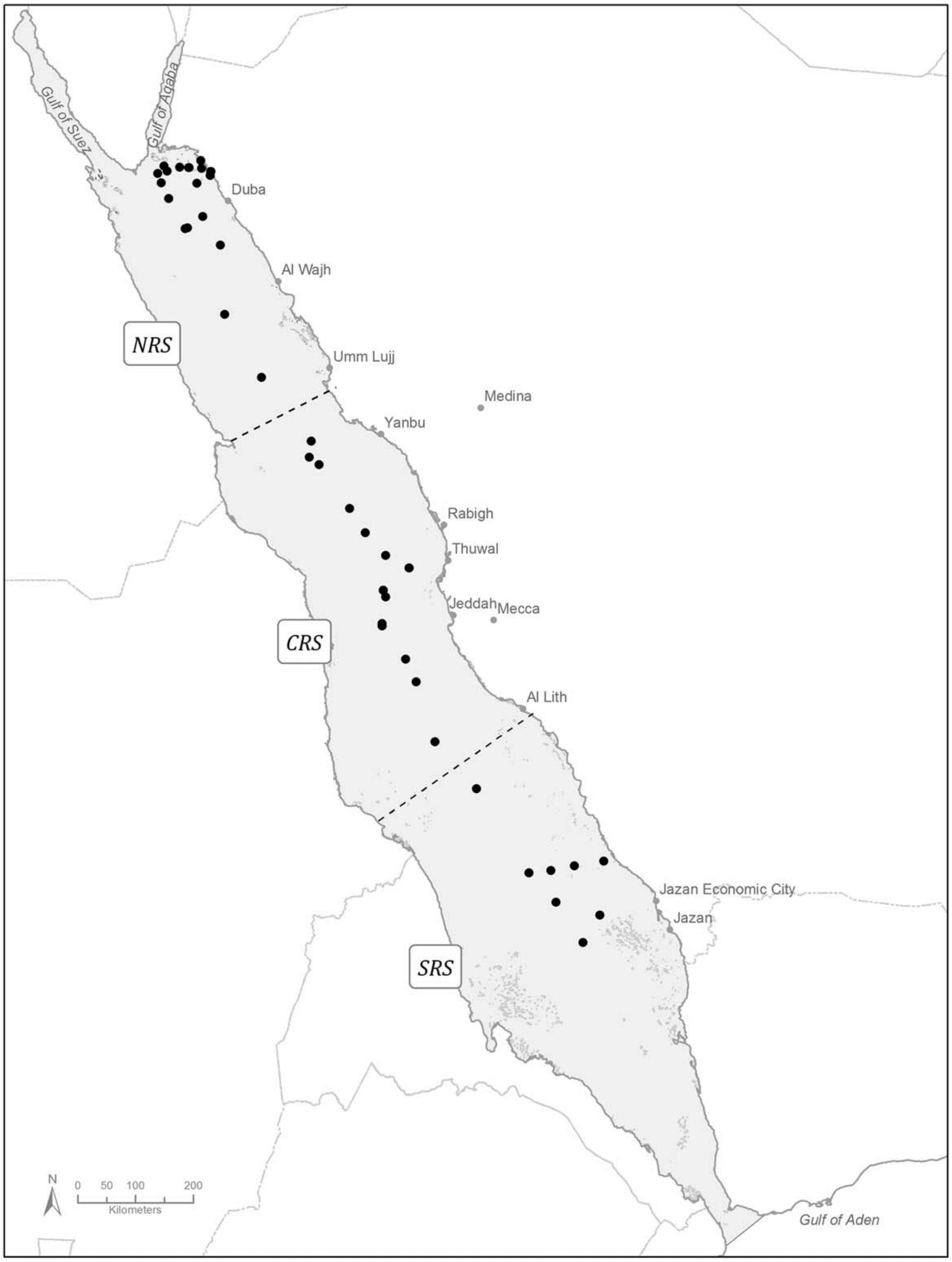

Figure 1. Map showing the locations of stations sampled during five cruises between October 2014 and January 2016 in the Red Sea (see Table 1). The delineation of the Northern Red Sea (NRS), the Central Red Sea (CRS), and the Southern Red Sea (SRS) is indicated on the map. Map produced using ArcGIS.

Table 1
Location and Dates of the Five Sampling Cruises in the Red Sea

Campaign	Platform	Location	Abbreviation	Period	Number of stations
Nutrient cycle cruise 1	RV *Thuwal*	Central Red Sea	CRS-01	16–28 Oct 2014	8
Jazan cruise	RV *Thuwal*	Southern Red Sea	Jazan	8–21 Feb 2015	8
Duba cruise 1	RV *Thuwal*	Northern Red Sea	Duba-01	17–28 Apr 2015	10
Duba cruise 2	RV *Thuwal*	Northern Red Sea	Duba-02	21 Mar to 2 Apr 2016	8
Nutrient cycle cruise 4	RV *Thuwal*	Central Red Sea	CRS-04	17–28 Jan 2016	6
Total					40

Central Red Sea (CRS) during fall and winter, specifically from 16 to 28 October 2014 and from 17 to 28 January 2016, respectively. Two cruises, Duba-01 and Duba-02 were conducted in the Northern Red Sea (NRS) in spring during the periods of 17–28 April 2015 and 21 March to 2 April 2016, respectively. A cruise to Jazan took place in the Southern Red Sea (SRS) in winter from 8 to 21 February 2015. A total of 40 stations were sampled: 18 in the NRS, 14 in the CRS, and 8 in the SRS (Figure 1 and Table 1).

Discrete seawater samples for determining phytoplankton pigment concentrations and particulate absorption spectra were collected using a rosette system equipped with 10 L Niskin bottles at typically 10 depths within the upper 200 m depth of the water column (5, 10, 20, 40, 50, 60, 70, 80, 150, and 200 m). Temperature and salinity profiles were obtained using a SBE 9 (Sea-Bird Electronics) conductivity-temperature-depth (CTD) probe. The data set consisted of 297 measurements of absorption spectra and phytoplankton pigment concentrations. The first optical depth, that corresponds to the surface layer observed by satellite ocean color sensors (Gordon & McCluney, 1975), was obtained as the euphotic depth, Ze, divided by 4.6 (Morel, 1988). Ze is the depth at which PAR decreases to 1% of its value ($\ln(1\%) = -4.6$) just below the sea surface and was derived from [TChl *a*] concentration profiles (Morel & Maritorena, 2001).

2.2. Phytoplankton Pigment Analysis

Seawater samples (with volume ranging from 2.3 to 2.8 L) were filtered through 25 mm diameter Whatman GF/F filters (0.7 μm porosity), stored in liquid nitrogen during the cruise and subsequently at -80°C in the laboratory until analysis. A total of 25 pigments were quantified using a high-performance liquid chromatography (HPLC) complete 1260 Agilent Technologies system according to the protocol described in Ras et al. (2008). Briefly, filters were ground in 3 mL of 100% methanol together with glass beads of 1 mm diameter by cell homogenizer. The extract was centrifuged for 10 min at 7,500 rpm and cooled at -5°C. Then the supernatants were filtered through a Teflon syringe filter of 0.2 μm and the extracts were analyzed.

In this study, the sum of concentrations of chlorophyll *a*, divinyl chlorophyll *a*, chlorophyllide *a*, and phaeo was used as an index of phytoplankton biomass and noted [TChl *a* + phaeo]. The term phaeo includes the sum of phaeophytin *a* and phaeophorbide *a* pigments. The total chlorophyll *b* concentration, noted [TChl *b*], and the total chlorophyll *c* concentration, noted [TChl *c*], were computed as the sum of the concentrations of chlorophyll *b* and divinyl chlorophyll *b* and chlorophyll *c*1, *c*2 and *c*3, respectively. Photosynthetic carotenoids (PSC) correspond to the sum of fucoxanthin (Fuco), peridinin (Peri), 19′-hexanoyloxyfucoxanthin (19′HF), and 19′-butanoyloxyfucoxanthin (19′BF), while nonphotosynthetic carotenoids (PPC) include zeaxanthin (Zea), alloxanthin (Allo), diadinoxanthin (Diadi), diatoxanthin (Diato), β-carotene, lutein (Lut), violaxanthin (Viola), and neoxanthin (Neo).

2.2.1. Estimation of Phytoplankton Size Based on Pigments

Diagnostic accessory pigments considered as biomarkers of specific phytoplankton taxonomic groups and size classes (Vidussi et al., 2001) were used to determine the relative proportions of picophytoplankton (<2 μm), nanophytoplankton (2–20 μm), and microphytoplankton (>20 μm). The biomass proportions associated with each size class were computed from pigment ratios following Uitz et al. (2006):

$$\%\text{micro} = 100 \times (1.41[\text{Fuco}] + 1.41[\text{Peri}])/\text{DP} \tag{1}$$

$$\%\text{nano} = 100 \times (0.6[\text{Allo}] + 1.27[19'\text{HF} - \text{Fuco}] + 0.35[19'\text{BF} - \text{Fuco}])/\text{DP} \tag{2}$$

$$\%\text{pico} = 100 \times (0.86[\text{Zea}] + 1.01[\text{TChl } b])/\text{DP} \quad (3)$$

where DP is the sum of the seven diagnostic pigment concentrations:

$$\text{DP} = 1.41[\text{Fuco}] + 1.41[\text{Peri}] + 0.6[\text{Allo}] + 0.35[19\text{¢BF}-\text{Fuco}] + 1.27[19'\text{HF-Fuco}] + 0.86[\text{Zea}] + 1.01[\text{TChl } b] \quad (4)$$

This approach has notable limitations. Some diagnostic pigments are shared by several phytoplankton groups and some groups may cover a broad size range, such as zeaxanthin containing *Trichodesmium* (microphytoplankton), or 19′BF and 19′HF in some picoplankton prymnesiophytes. This approach is not compared with others techniques such as flow cytometry, microscopy, and molecular analysis. However, several previous studies demonstrated good performances of this method in providing the dominant trends of the phytoplankton community size structure in other oligotrophic regions of the world's oceans (Organelli et al., 2013; Ras et al., 2008; Uitz et al., 2008, 2015).

The size index (SI) was derived from the proportions of picophytoplankton, nanophytoplankton, and microphytoplankton to provide a single indicator of the dominant phytoplankton community size structure (Bricaud et al., 2004). SI was computed as follows:

$$\text{SI} = (1 \times [\%\text{pico}] + 5 \times [\%\text{nano}] + 50 \times [\%\text{micro}])/100 \quad (5)$$

where 1, 5, and 50 μm are taken as central size values for each phytoplankton class (Bricaud et al., 2004).

2.3. Particulate Absorption Measurements

Particulate absorption spectra, $a_p(\lambda)$, were measured using a quantitative filter pad technique (Mitchell et al., 2003). Seawater samples (2.3–2.8 L) were filtered on Whatman GF/F filters (0.7 μm porosity) and stored in liquid nitrogen during the cruise and subsequently at $-80°$C in the laboratory until analysis. Particulate absorption spectra were measured, with a Varian Cary 5000 double-beam ultraviolet-visible-infrared spectrophotometer equipped with an integrating sphere, in the 300–800 nm spectral range at 1 nm intervals. A blank wet filter (pure water) was used as a reference. We used this equipment with samples placed inside the integrating sphere, which allowed us to minimize the scattering error and to determine whether significant absorption exists in the near infrared. All spectra were converted into $a_p(\lambda)$ (in m^{-1}) and then corrected for the path length amplification effect according to Stramski et al. (2015).

The respective contributions of phytoplankton ($a_{ph}(\lambda)$) and nonalgal particles ($a_{nap}(\lambda)$) to total particulate absorption were determined by numerical decomposition (Bricaud & Stramski, 1990).

A few samples ($N = 21$) were also analyzed using the method of Kishino et al. (1985), based on the pigment extraction in methanol. Absorption ratios derived from these $a_{ph}(\lambda)$ spectra were found to be very close to the standard ratios used in the numerical decomposition. In addition, the comparison between $a_{ph}(\lambda)$ and $a_{nap}(\lambda)$ spectra obtained using the method of Kishino et al. (1985) and those estimated from numerical decomposition was high ($R^2 = 0.96$, slope = 1.03; $R^2 = 0.88$, slope = 1.08; $N = 21$, $p < 0.0001$, respectively) confirming the validity of the method established by Bricaud and Stramski (1990) for Red Sea waters.

Pigment-specific values of phytoplankton absorption coefficients, $a_{ph}^*(\lambda)$, were computed by dividing $a_{ph}(\lambda)$ by [TChl *a*].

2.4. Estimation of Phytoplankton Size Based on the Phytoplankton Absorption Spectrum

An estimation of the phytoplankton size factor, S_f, was computed based on the shape of the phytoplankton absorption spectrum as described by Ciotti et al. (2002). The model developed by Ciotti et al. (2002) reconstructs the shape of any phytoplankton absorption spectrum (normalized by the mean in the 400–700 nm range) using a linear combination of two spectra corresponding to pure picophytoplankton and microphytoplankton populations. Note that the picophytoplankton vector used here was provided by Ciotti and Bricaud (2006). The values of S_f vary from 0 to 1. S_f tends to 0 for a population composed exclusively of microphytoplankton and to 1 for a pure picophytoplankton assemblage. Values of S_f comprised between 0 and 1 represent all possible conditions between these two extremes. The accuracy of the spectral fit was assessed for each phytoplankton absorption spectrum by computing the coefficient of correlation, R^2, between all spectral values and those reconstructed by the model. Values of S_f corresponding to $R^2 \geq 0.97$ (RMSE = 0.073 ± 0.022) between measured and reconstructed phytoplankton absorption spectra were retained (92% of the entire database).

3. Results and Discussion

3.1. Particulate, Phytoplankton, and Nonalgal Particles Absorption Coefficients as a Function of [TChl *a*]

Variations of $a_p(\lambda)$, $a_{ph}(\lambda)$, and $a_{nap}(\lambda)$ as a function of [TChl *a*] are displayed in Figures 2 and 3 and are compared with the global relationships established for oligotrophic waters using in situ measurements in various regions of the global ocean. With reference to ocean color remote sensing, the analyses of $a_p(\lambda)$, $a_{ph}(\lambda)$, and $a_{nap}(\lambda)$ as a function of [TChl *a*] was also restricted to the first optical depth. The regression formula in the form of a power law for each relationships between the parameter of interest and [TChl *a*] are presented in Table 2.

3.1.1. Particulate Absorption Coefficients as a Function of [TChl *a*]

The a_p values at 440 and 676 nm within the surface layer are significantly correlated to [TChl *a*] ($R^2 = 0.87$ and 0.89, respectively, $N = 108$, $p < 0.0001$) as well as when considering all samples from the upper 200 m depth ($R^2 = 0.85$ and 0.88, respectively, $N = 297$, $p < 0.0001$) (Figures 2a and 2b). The $a_p(\lambda)$ versus [TChl *a*] relationships obtained using measurements limited to the first optical depth significantly differ from those established when all depths were considered ($p < 0.05$ for all, ANCOVA test). We also found that our measurements, which were collected both within the surface layer and in all depths, were slightly higher for a given [TChl *a*] than those of Bricaud et al. (1998), for the global ocean, and Brewin et al. (2015), for the Red Sea, over the whole range of our measurements ([TChl *a*] = 0.006 to 1 mg m^{-3}) (Figures 2a and 2b).

The relationships obtained using measurements limited to the surface layer differ statistically with those established when all depths were considered ($p < 0.05$ for all, ANCOVA test). We found that our

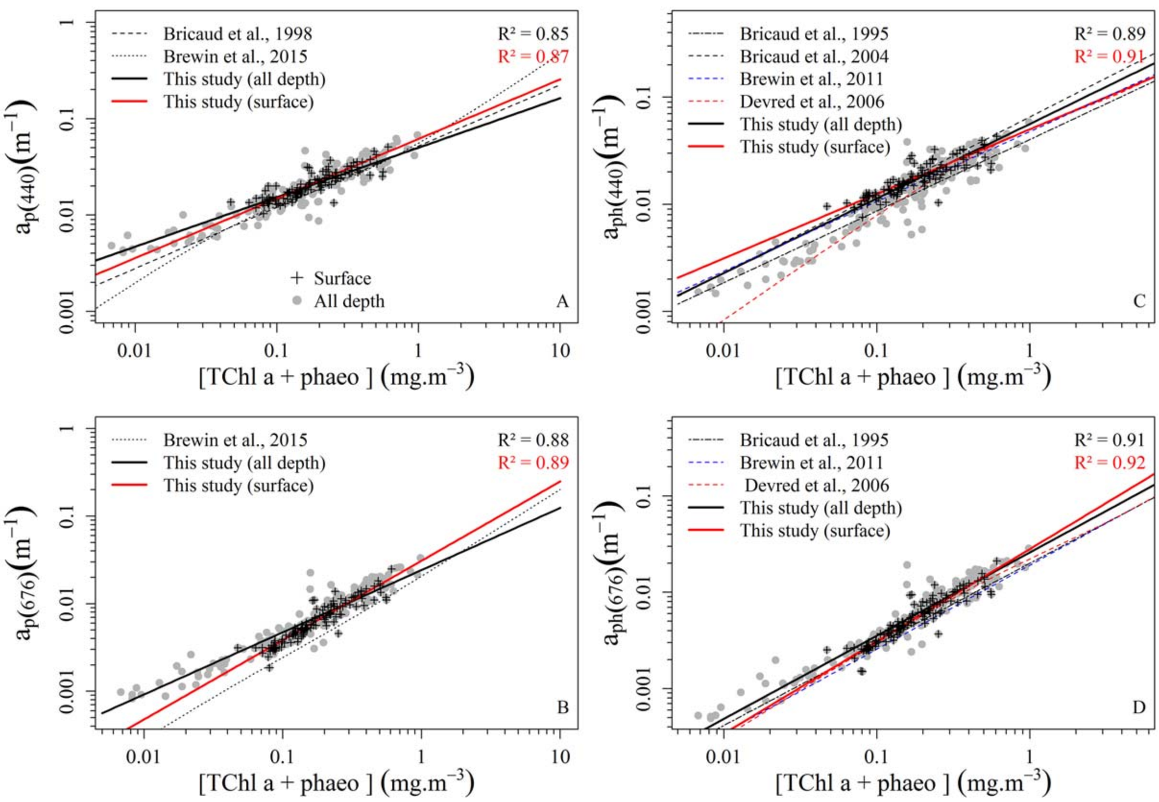

Figure 2. Variations of the particulate absorption coefficients (a) at 440 nm, $a_p(440)$ and (b) at 676 nm, $a_p(676)$, as a function of [TChl *a*]. The black and red solid lines represent the best fit (power law function) between $a_p(\lambda)$ and [TChl *a*] in all depths and within the first optical depth, respectively. The relationships from Bricaud et al. (1998) (dashed line) and Brewin et al. (2015) (dotted line) are displayed. Variations of the phytoplankton absorption coefficients (c) at 440 nm, $a_{ph}(440)$, and (d) at 676 nm, $a_{ph}(676)$, as a function of [TChl *a*]. The black and red solid lines represent the best fit (power law function) between $a_{ph}(\lambda)$ and [TChl *a*] in all depths and within the first optical depth, respectively. The relationships from Bricaud et al. (1995) (dashed-dotted line), Bricaud et al. (2004) (dashed line), Devred et al. (2006) (red dashed line), and Brewin et al. (2011) (blue dashed line) are displayed. The version of $a_{ph}(676)$ as a function of [TChl *a*] was not provided by Bricaud et al. (2004). The relationships of Devred et al. (2006) and Brewin et al. (2011, 2015) are for 443 and 670 nm rather than 440 and 676 nm.

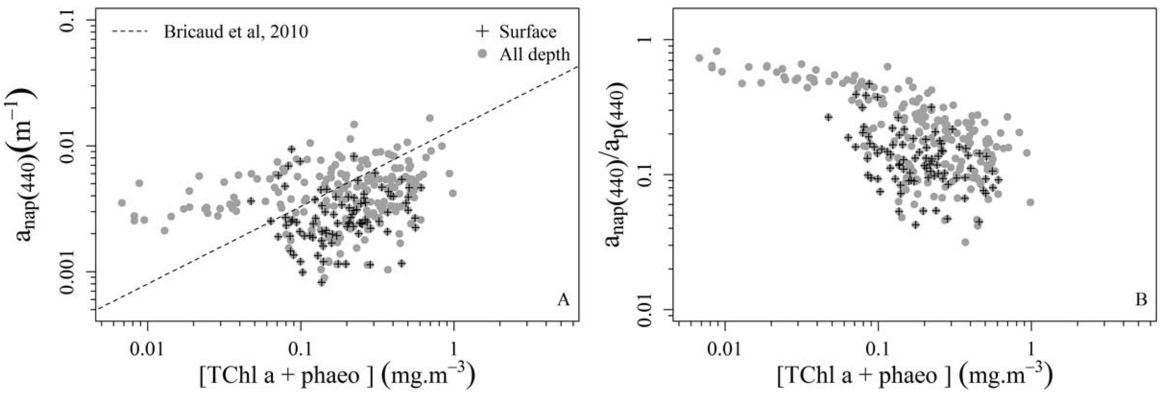

Figure 3. (a) Variations of the absorption coefficient of nonalgal particles at 440 nm, $a_{nap}(440)$, as a function of [TChl *a*]. The relationship provided by Bricaud et al. (2010) is displayed. (b) Variations the nonalgal to particulate absorption ratio, a_{nap}/a_p at 440 nm as a function of [TChl *a*].

measurements, which have been collected both within the surface layer and in all depths, were slightly above those of Bricaud et al. (1998), for the global ocean, and Brewin et al. (2015), for the Red Sea, over the whole range of our measurements ([TChl *a*] = 0.006–1 mg m^{-3}) (Figures 2a and 2b).

Possible reasons for the differences between our results and those of Brewin et al. (2015) may be attributed to the use of HPLC-measured [TChl *a*] in this study. Brewin et al. (2015) obtained [TChl *a*] from a_p measurements at 650, 676, and 715 nm (Line Height method) in Red Sea waters. Although this method has been found to perform well in various areas of the global ocean (Boss et al., 2007, 2013b; Dall'Olmo et al., 2009, 2012; Roesler & Barnard, 2013; Westberry et al., 2010), our results show that a linear fit to our data of [TChl *a*] measured by HPLC versus [TChl *a*] retrieved from $a_p(\lambda)$ provided the equation [TChl $a]_{LH} = 1.17 \times$ [TChl $a]_{HPLC} + 0.0026$ ($R^2 = 0.91$, $N = 297$, $p < 0.0001$) was not apparent, indicating significant overestimation of [TChl $a]_{LH}$ as compared with [TChl $a]_{HPLC}$. Furthermore, Brewin et al. (2015) used a larger number of measurements of $a_p(\lambda)$ below 0.1 mg m^{-3} compared to our data set, which could also affect the conclusions in our study.

3.1.2. Phytoplankton Absorption Coefficients as a Function of [TChl *a*]

The relationships between a_{ph} and [TChl *a*] at 440 and 676 nm are shown in Figures 2c and 2d. A significantly high correlation is also found between $a_{ph}(\lambda)$ and [TChl *a*] within the surface layer and among depths at 440 nm ($R^2 = 0.89$ and 0.91, $N = 108$ and 297, respectively, $p < 0.0001$) and at 676 nm ($R^2 = 0.91$ and 0.92, $N = 108$ and 297, respectively, $p < 0.0001$). As for $a_p(\lambda)$, the relationships between $a_{ph}(\lambda)$ and [TChl *a*] established within the surface waters significantly differ from those established considering all samples between 0 and 200 m depth ($p < 0.05$ for both, ANCOVA test).

Table 2
Results From the Regression[a] Analysis Between $a_p(440)$, $a_p(676)$, $a_{ph}(440)$, $a_{ph}(676)$, and [TChl a] Among All Depths and Within the Surface Layer Presented in Figure 2

		$a_p(440)$	$a_p(676)$	$a_{ph}(440)$	$a_{ph}(676)$
All depths	A	0.05	0.024	0.056	0.026
	B	0.51	0.71	0.70	0.87
	R^2	0.85	0.88	0.89	0.91
	N		*297*		
Surface	A	0.062	0.031	0.050	0.028
	B	0.62	0.90	0.60	0.96
	R^2	0.87	0.89	0.91	0.92
	N		*108*		

[a]The regression formula is in the form of a power law as X = A [TChl $a]^B$ where A and B are the best fit parameters. The determination coefficient, R^2, and the number of data, *N*, are also shown. All regressions are significant for $p < 0.0001$.

The relationships obtained between $a_{ph}(\lambda)$ and [TChl *a*] within the surface as well as along the water column are above the existing global relationships proposed by Bricaud et al. (1995), Devred et al. (2006), and Brewin et al. (2011) (Figures 2c and 2d) ($p < 0.05$ for all, ANCOVA test). Given the relationships established by Devred et al. (2006) and Brewin et al. (2011) are based on a two-population model and not on a power law function, this may affect our comparisons in this study. Indeed, these models relate $a_{ph}(\lambda)$ to [TChl *a*], assuming that the assemblages of phytoplankton comprise mixtures of two populations whose proportions vary as the total concentration of cells changes. On the other hand, the relationship obtained at 440 nm considering all depths is in relatively good agreement with the relationship determined by Bricaud et al. (2004) (Figure 2c) ($p \geq 0.05$, ANCOVA test), although this relationship is only representative of measurements collected in the surface layer. The relationship of Bricaud et al. (2004) is based on a different data set (measurements collected in various oceanic regions and trophic states) than the one used in Bricaud et al.

(1995) and might explain why the relationship of Bricaud et al. (2004) is more closely aligned to the relationship revealed in this study.

3.1.3. Nonalgal Particles Absorption Coefficients as a Function of [TChl *a*]

No clear relationship between a_{nap} at 440 nm and [TChl *a*] appears among depths (Figure 3a). This is in agreement with previous studies performed in oligotrophic waters (Cleveland, 1995). The $a_{nap(440)}$ values are highly scattered around the relationship established by Bricaud et al. (2010) from data collected in the Pacific Ocean (BIOSOPE area), reflecting different trophic regimes. Furthermore, in the deep layer where [TChl *a*] varies from 0.006 to 0.1 mg m^{-3}, $a_{nap}(440)$ values are higher than those predicted by this relationship (Figure 3a). The ratio of nonalgal absorption coefficient to particulate absorption at 440 nm, $a_{nap}(440)/a_p(440)$, as a function of [TChl *a*] is displayed in Figure 3b. Deep Red Sea waters with low [TChl *a*] concentrations (0.006–0.1 mg m^{-3}) are characterized by high values of $a_{nap}(440)/a_p(440)$, between 0.45 and 1. This result suggests that the $a_{nap}(440)/a_p(440)$ varies inversely to [TChl *a*] in clear Red Sea waters. This is consistent with the observations made in other oligotrophic regions, such as in the Pacific Ocean (Bricaud et al., 2010). Bricaud et al. (2010) suggested that the high contribution of the $a_{nap}(440)/a_p(440)$ ratio could indicate the presence of a large amount (or more colored) of nonalgal particles. The Red Sea is also known as a region where significant inputs from dust occur (Al-Taani et al., 2015; Ginoux et al., 2012; Prakash et al., 2015; Prospero et al., 2002). Frequent dust outbreaks and dust storms have been observed in the Red Sea during our research cruises. Satellite observations (http://neo.sci.gsfc.nasa.gov/view.php?datasetId=MODAL2_M_AER_OD) revealed that Saharan dust events occurred in the entire Red Sea during most of the cruises (CRS-04, Duba-01, Duba-02, and Jazan) performed for this study. The presence of these inorganic particles can partly explain the high contribution of the $a_{nap}(440)/a_p(440)$ ratio in Red Sea deep waters by increasing the sinking velocity of nonalgal particles (Ploug et al., 2008). When [TChl *a*] varies from 0.1 to 1 mg m^{-3}, $a_{nap}(440)/a_p(440)$ is highly variable with values ranging from 0.028 to 0.45. This is consistent with the values observed in the Pacific Ocean, Mediterranean Sea, and Atlantic Ocean (Bricaud et al., 2010). This large variability can be explained by varying contributions of nonalgal particles (detritus, bacteria, viruses, and inorganic particles) along the water column. Several studies also demonstrated that dust inputs have a positive effect on bacterial growth and abundance, diversity, and composition of the indigenous bacterial assemblages (Reche et al., 2009; Lekunberri et al., 2010; Morales-Baquero et al., 2013). Dust deposition can thus affect the proportion of bacteria in Red Sea waters and partly explain the high variability observed in the $a_{nap}(440)/a_p(440)$ ratio.

The above comparisons suggest that the high values of $a_p(\lambda)$ observed within the surface Red Sea waters ([TChl *a*] below 0.1 mg m^{-3}) is mainly related to an important contribution of nonalgal particles in these waters (Figures 2a and 2b).

3.2. Phytoplankton Size Structure Associated With Phytoplankton Absorption Spectra

Variability in $a_{ph}(\lambda)$ is observed in this study (Figures 2c and 2b). The variability observed around the relationship between $a_{ph}(\lambda)$ and [TChl *a*] may be due to changes in phytoplankton community structure. It is generally known that variations in phytoplankton size structure and the intracellular concentrations of diverse phytoplankton pigments induce variations in $a_{ph}(\lambda)$ at a given [TChl *a*] (Bricaud et al., 2004, 2010; Ferreira et al., 2013; Organelli et al., 2011; Sathyendranath et al., 1996).

The relative contributions of nano- and picophytoplankton to total algal biomass are high in Red Sea waters (Figure 4). Based on phytoplankton pigment ratios, we found that picophytoplankton dominate the upper layer in the whole basin due to the presence of *Prochlorococcus* sp and *Synechococcus* sp, but it remains highest in the central part of the basin (>60% of the phytoplankton biomass). The nanophytoplankton group, mainly associated with prymnesiophytes and pelagophytes, is relatively abundant (40–60% of the phytoplankton biomass) below 25 m depth to 180 m depth along the whole basin. The microphytoplankton pool, primarily associated with diatoms, is mainly observed in the southern part (45–75% of phytoplankton biomass) of the basin and were present in low concentrations (5–30% of the total phytoplankton biomass) in the other bioregions (not shown). These observations are consistent with the phytoplankton community size structure generally found in oligotrophic areas of the ocean (Bricaud et al., 2004; Organelli et al., 2011; Ras et al., 2008) and in the Red Sea (Kheireddine et al., 2017; Pearman et al., 2016). As this trend has been discussed in details in Kheireddine et al. (2017) where they studied the spatiovertical distribution of phytoplankton pigments during similar time periods (Jazan and Duba-01 cruises) or season of sampling, the

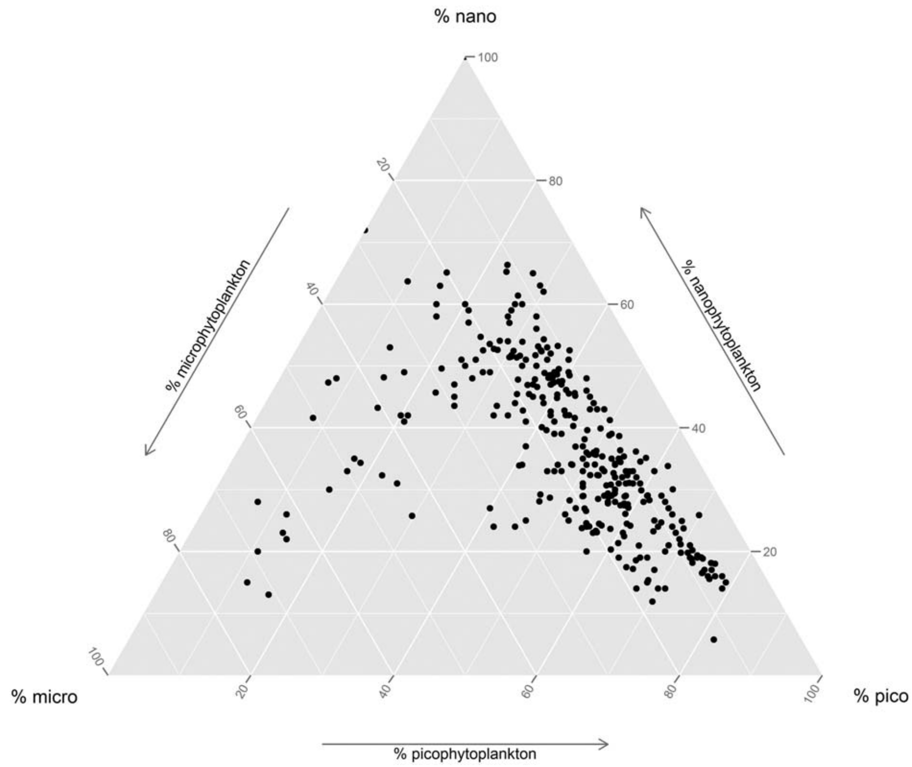

Figure 4. Relative proportions (%) of microphytoplankton, nanophytoplankton and picophytoplankton estimated from the relative concentrations of some diagnostic pigments (equations (1)–(3)). For each sample, the relative contribution of a size class to total biomass can be read on the corresponding axis as indicated.

reader is referred to Kheireddine et al. (2017) and references therein for more information regarding the phytoplankton community size structure distributions in the Red Sea.

To examine variations in the shape of the phytoplankton absorption spectra of each phytoplankton size class (microphytoplankton, nanophytoplankton, and picophytoplankton), spectra are normalized to its mean value computed on the basis of all spectral values between 400 and 700 nm (Ciotti et al., 2002), and then grouped into the three size classes according to dominance (>50%).

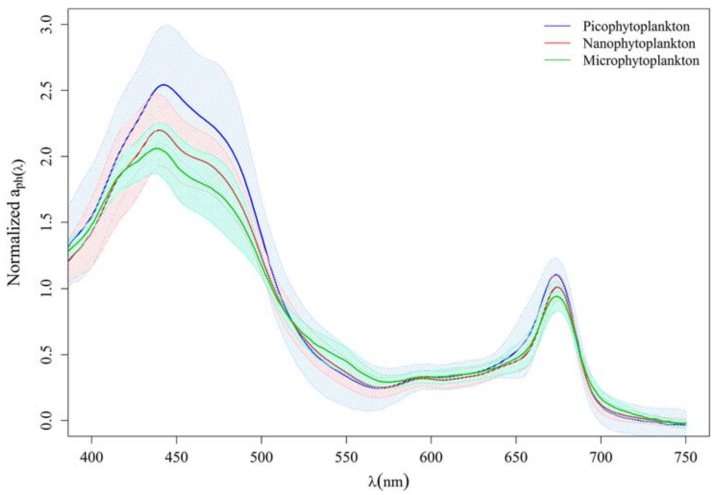

Figure 5. Average of phytoplankton absorption spectra normalized by the average value of absorption between 400 and 700 nm shown separately for picophytoplankton-dominated samples (blue solid line), nanophytoplankton-dominated samples (red solid line), and microphytoplankton-dominated samples (green solid line). For each group of data, the mean normalized spectrum (solid line) and the standard deviation (dashed area) are displayed.

Differences between the average spectra for each dominant community size of phytoplankton can be observed (Figure 5). For the picophytoplankton-dominated spectra, the blue-to-red ratio is higher (2.35) than in nanophytoplankton (2.21) or microphytoplankton (2.16) dominated spectra. This result reflects a stronger package effect for microphytoplankton cells. This is in agreement with previous studies showing that variability in the spectral shape of phytoplankton absorption can be mainly attributed to changes in phytoplankton cell size (Brewin et al., 2011; Ciotti et al., 2002; Devred et al., 2006; Lohrenz et al., 2003; Sathyendranath et al., 2001; Wang et al., 2015). Note that the variations around the mean spectra of picophytoplankton-dominated absorption coefficients reflect a larger variability in the contribution of accessory pigments associated with smaller cells in comparison to those dominated by microphytoplankton (Figure 5).

Ciotti et al. (2002) showed that in the surface layer, the variability in the spectral shape of phytoplankton absorption could be mainly explained by variation in cell size of the major phytoplankton group,

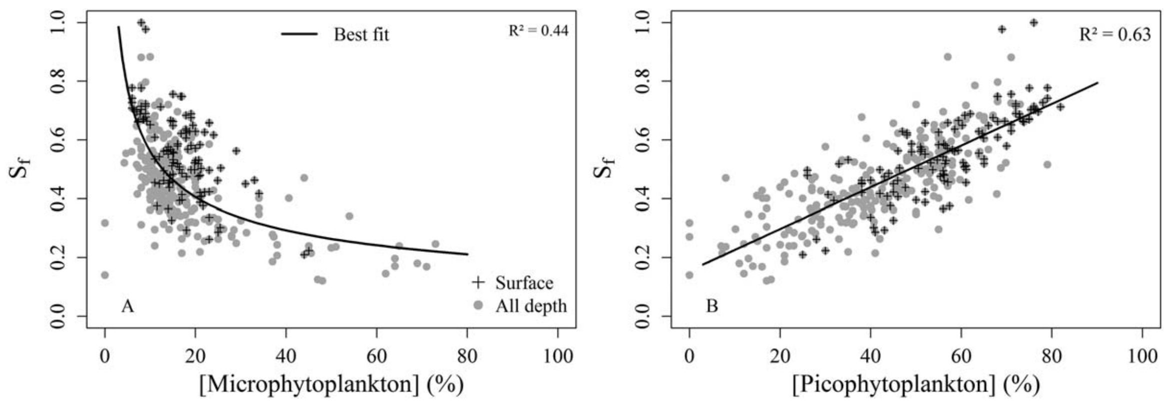

Figure 6. Variations of the cell size parameter (S_f) derived from the shape of the phytoplankton absorption spectrum as described by Ciotti et al. (2002) as a function of the proportions (%) of (a) microphytoplankton and (b) picophytoplankton estimated from the relative concentrations of some diagnostic pigments (equations (1)–(4)). The coefficient of determination was calculated on the basis of all data in the form (a) of a power law and (b) of a linear regression.

thus enabling the development of a model to estimate a cell size parameter for phytoplankton (i.e., S_f). In the present study we estimated S_f for each phytoplankton absorption spectrum. The model of Ciotti et al. (2002) provides estimates of the dominant size of the phytoplankton community that can be compared to the relative proportions of picophytoplankton and microphytoplankton that are derived from phytoplankton diagnostic pigments (see methods; Bricaud et al., 2004; Uitz et al., 2006; Vidussi et al., 2001). The values of S_f vary from 0.12 to 0.98 (Figure 6).

S_f decreases when the contribution of microphytoplankton tends to increase (Figure 6a) and increases with the proportion of picophytoplankton (Figure 6b). S_f values are in good agreement with the relative proportion of picophytoplankton ($R^2 = 0.63$, $N = 297$, $p < 0.0001$) and microphytoplankton ($R^2 = 0.44$, $N = 297$, $p < 0.0001$) despite the scattering observed around these relationships due to the photoacclimation of phytoplankton cells in depth. It is well established that the proportion in accessory pigments vary along the water column (Bricaud et al., 1995; Organelli et al., 2011). For example, photoprotective pigments tend to a continuously decrease from the surface to deeper waters (Bricaud et al., 1995; Kheireddine et al., 2017; Organelli et al., 2011). This can significantly impact the shape of the phytoplankton absorption spectrum. As the model of Ciotti et al. (2002) was established for surface waters, its use for samples collected in depth could reveal photoacclimation responses to the vertical light variation. For example, for the same dominant cell size, the S_f values will tend to decrease if the phytoplankton community shows an increase in the concentrations of intracellular pigments caused, for instance, by photoacclimation (Ciotti et al., 1999).

The scattering observed around these relationships could also be partly explained by the fact that the phytoplankton community size is inferred by phytoplankton pigments that may be shared by several phytoplankton size class as mentioned previously. Overall, considering the assumptions in each approach, these results suggest that the absorption-based method developed by Ciotti et al. (2002) is consistent with the approach based on phytoplankton pigments.

3.3. Specific Phytoplankton Absorption Variability Associated With Changes in Phytoplankton Cell Size and Pigment Composition

As reported in previous studies (Allali et al., 1997; Bricaud et al., 1995, 2004; Ferreira et al., 2013; Organelli et al., 2011; Sathyendranath et al., 1996), a_{ph}* values clearly decrease with increasing [TChl *a*] at 440 nm within the surface layer and among depths ($R^2 = 0.61$, $N = 108$ and 297, respectively, $p < 0.0001$), and slightly decrease at 676 nm only when all depth are considered ($R^2 = 0.44$, $N = 297$, $p < 0.0001$) (Figure 7). A broad range of variation in [TChl *a*] (0.008–1 mg m^{-3}) is associated with a narrower variability in a_{ph}*(676) values (0.011–0.036 m^{-1}), whereas a_{ph}*(440) values vary widely (0.029–0.152 m^{-1}). This observation is consistent with anterior studies in other oligotrophic environments (Bouman et al., 2003; Organelli et al., 2011; Perez et al., 2007; Vijayan & Somayajula, 2014). The large variability observed in a_{ph}*(440) and a_{ph}*(676) for a given [TChl *a*] can be attributed to changes in phytoplankton community size structure and pigment composition. The estimations of S_f may help in explaining the variability observed around the relationship between a_{ph}*(λ) and [TChl *a*] (Figure 7). In general, the highest a_{ph}*(λ) correspond to higher S_f values

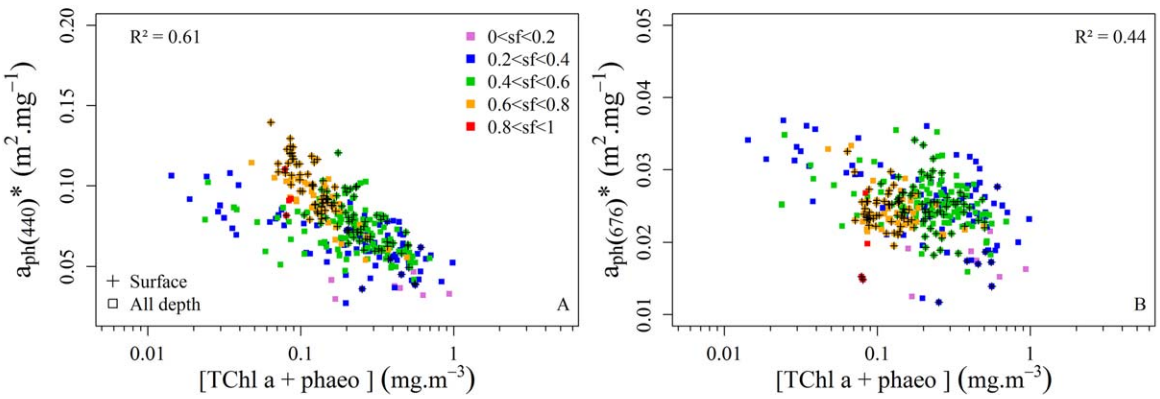

Figure 7. Variations of chlorophyll-specific phytoplankton absorption coefficients (a) at 440 nm, $a_{ph}(440)^*$, and (b) at 676 nm, $a_{ph}(676)^*$, as a function of [TChl *a*]. Samples are grouped for different ranges of cell size parameter (S_f) as indicated in the legend. The coefficient of determination was calculated on the basis of all data in the form of a power law.

(smaller phytoplankton cell size), and the lower $a_{ph}^*(\lambda)$ to the lower S_f values (larger phytoplankton cell size) (Figure 7). This is in agreement with the literature (Brunelle et al., 2012; Ferreira et al., 2013; Lohrenz et al., 2003; Roy et al., 2011; Sathyendranath et al., 1999; Stuart et al., 1998; Wang et al., 2015) and reflects an increasing pigment packaging effect with increasing [TChl *a*] and the dominance of larger phytoplankton cell sizes (Barlow et al., 2008; Bricaud et al., 1995; Morel et al., 2006). Nevertheless, some S_f values ($0.2 < S_f < 0.4$) above the surface layer are not consistent with the general assumption of increasing S_f with increasing $a_{ph}^*(\lambda)$ (Figure 7). These S_f values are observed for a large variation in [TChl *a*] that does not conform with the general assumption that S_f values decrease with increasing [TChl *a*] (Ciotti et al., 2002) in response to photoacclimatation processes (Figure 7). Indeed, such inconsistencies can occur because S_f does not depend only on cell size. It reflects changes in pigment composition and package effect in response to changes in phytoplankton cell size associated with variations in intracellular pigment content from surface to deep waters that affect the spectral shape of phytoplankton absorption (Ciotti et al., 2002; Morel & Bricaud, 1981). For example, Ferreira et al. (2013) have shown that, for the same phytoplankton cell size, S_f values tend to decrease if phytoplankton community shows an increase in the concentrations of intracellular pigments due to photoacclimation (Ciotti et al., 1999). Thus, the parameter S_f cannot be used solely to study changes in phytoplankton cell size as variations in intracellular pigment content will also affect this parameter at a given cell size (Ciotti et al., 1999). This result is not surprising because it is known that the shape of the phytoplankton spectrum is affected both by the cell size of the major phytoplankton groups and also by the intracellular pigment content (Morel & Bricaud, 1981).

3.3.1. Impact of Phytoplankton Cell Size on $a_{ph}^*(440)$

The importance of phytoplankton cell size in determining $a_{ph}^*(440)$ is displayed in Figure 8, in which $a_{ph}^*(440)$ is plotted as a function of the relative proportion in microphytoplankton (Figure 8a), nanophytoplankton (Figure 8b), picophytoplankton (Figure 8c), and S_f (Figure 8d). These relationships clearly show that the highest values of $a_{ph}^*(440)$ are found within the surface layer and are associated with small phytoplankton cell size (Figure 8). We show that only 18% of the variability in $a_{ph}^*(440)$ could be attributed to the microphytoplankton pool (mainly diatoms). The nanophytoplankton pool (prymnesiophytes and pelagophytes) can explain 28% of the variability in $a_{ph}^*(440)$ and the picophytoplankton pool (*Synechococcus* sp. and *Prochlorococcus* sp.) plays a significant role in changing $a_{ph}^*(440)$, controlling 44% of the variability (Figures 8a–8c). While we show that the S_f parameter is dependent not only on the phytoplankton size but also on the intracellular pigment content, we observe that S_f can explain 46% of the variation observed in $a_{ph}^*(440)$ (Figure 8d). It is well established that phytoplankton functional types (PFTs) correspond to phytoplankton species with similar biogeochemical roles and physiological traits and that the phytoplankton size distribution is a major defining trait of PFTs (Le Quéré et al., 2005). The size distribution is also known as a major factor determining particle sinking rates and thus their role in carbon export (Buesseler et al., 2007; Eppley et al., 1967; McCave, 1975; Stemmann et al., 2004). Therefore, in our study, we can consider that picophytoplankton, nanophytoplankton, and microphytoplankton are three PFTs according to their size distribution. Thus, our results confirm that variations in $a_{ph}(\lambda)$ can induce information about PFTs.

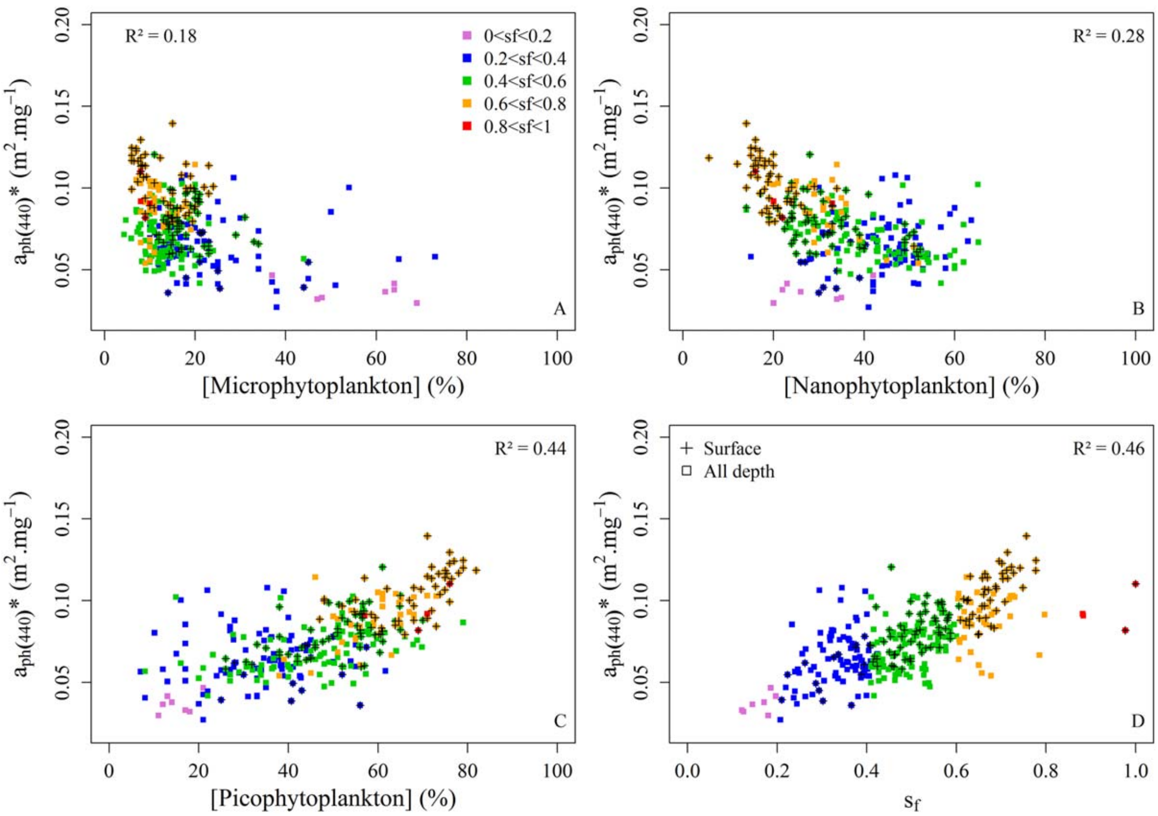

Figure 8. Variations of chlorophyll-specific phytoplankton absorption coefficients at 440 nm, $a_{ph}(440)^*$, as a function of the proportions (%) of (a) microphytoplankton, (b) nanophytoplankton, (c) picophytoplankton estimated from the relative concentrations of some diagnostic pigments (equations (1)–(3)) and (d) the cell size parameter (S_f) derived from the shape of the phytoplankton absorption spectrum as described by Ciotti et al. (2002). Samples are grouped for different ranges of cell size parameter (S_f) as indicated in the legend. The coefficient of determination was calculated on the basis of all data in the form of a power law (Figures 8a and 8b) and of a linear regression (Figures 8c and 8d).

3.3.2. Influence of Changes in Phytoplankton Pigment Composition on $a_{ph}^*(440)$

To examine the impact of changes in phytoplankton pigments composition on $a_{ph}^*(440)$, we chose to group the accessory phytoplankton pigments into four distinct categories: (1) [TChl *b*]; (2) [TChl *c*]; (3) PSC; and (4) PPC. The variability in $a_{ph}^*(440)$ as a function of the ratio of the four categories of accessory pigments, relatively to [TChl *a*], is examined (Figure 9). The [TChl *b*]/[TChl *a*] ratio within the surface layer mainly varies in a narrow range from 0 to 0.25 while a broad range of variation in $a_{ph}^*(440)$ at depth can be observed (Figure 9a), suggesting that changes in proportion of chlorophyll *b* and divinyl chlorophyll *b* play no significant role in the variability of $a_{ph}^*(440)$. The [TChl *c*]/[TChl *a*] ratio values vary from 0.03 to 0.35 (Figure 9b) in all depths and from 0.03 to 0.18 within the surface layer. The increase in the [TChl *c*]/[TChl *a*] ratio from 0 to 0.2 is accompanied by decreasing $a_{ph}^*(440)$ values (Figure 9b). Some [TChl *c*]/[TChl *a*] values deviate from this trend, notably measurements collected above the surface layer, for which the ratio is higher than 0.2. We show that only 24% of the variability in $a_{ph}^*(440)$ could be associated with the [TChl *c*]/[TChl *a*] ratio (Figure 9b). The [PSC]/[TChl *a*] ratio mainly varies from 0.2 to 0.5 within as well above the surface while $a_{ph}^*(440)$ show a more broad range of variations (Figure 9c). The points where [PSC]/[TChl *a*] ratio values are higher than 0.5 are the samples collected in the deeper layer. In many studies, it has been shown that photosynthetic accessory pigment concentrations can increase with increasing depth in response to lower light levels in deep waters (Bricaud & Stramski, 1990; Kirk, 1994; Majchrowski & Ostrowska, 2000). About 13% of the variability in $a_{ph}^*(440)$ is attributed to the [PSC]/[TChl *a*] ratio. Unlike the [PSC]/[TChl *a*] ratio, the [PPC]/[TChl *a*] ratio (mainly associated with zeaxanthin/[TChl *a*] in this study) varies in a broad range from 0 to 1.2 (Figure 9d). The highest [PPC]/[TChl *a*] values associated with smaller phytoplankton cell size (S_f varying from 0.6 to 1) are observed within the surface (Figure 9d), and this is consistent with those observed in other oligotrophic regions characterized by high light and low nutrient conditions (Barlow et al., 2004; Bricaud et al., 1995, 2004; Organelli et al., 2011; Sathyendranath et al., 2005; Stuart et al., 1998, 2004). Stuart

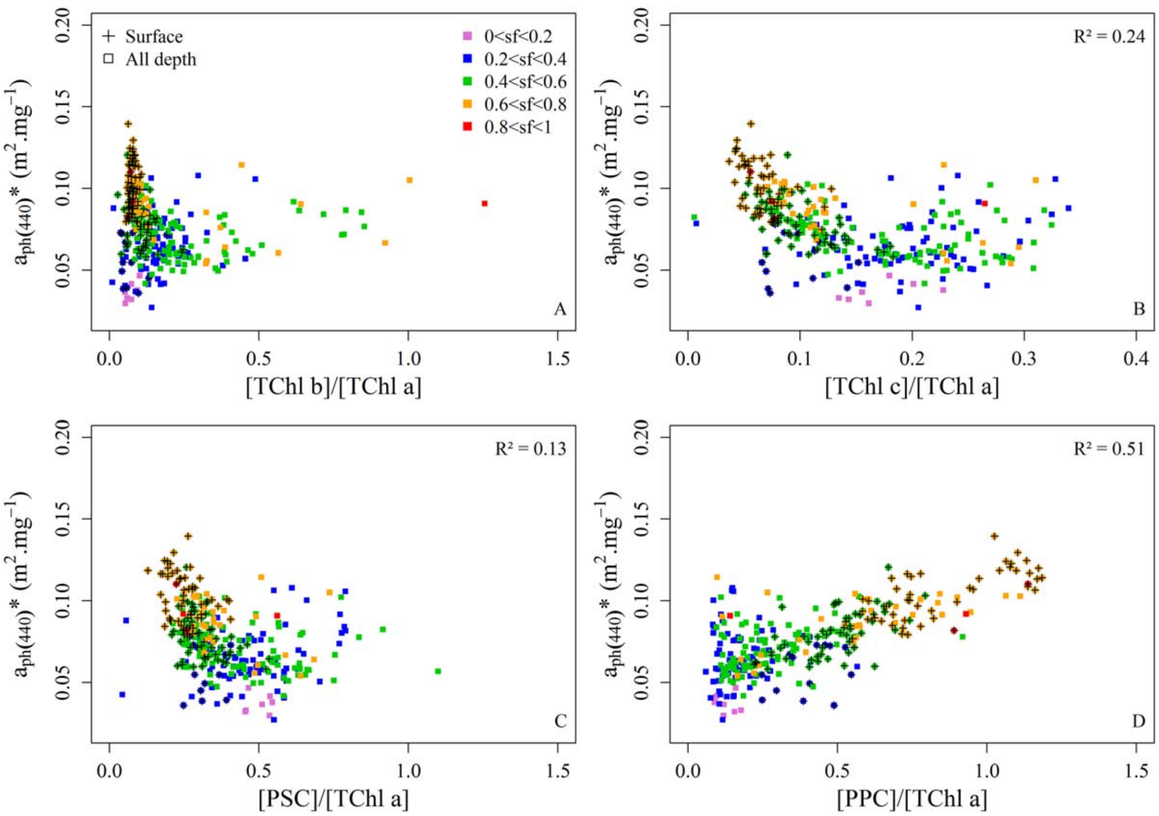

Figure 9. Variations of chlorophyll-specific phytoplankton absorption coefficients at 440 nm, $a_{ph}(440)^*$, as a function of the accessory pigments to [TChl *a*] ratios: (a) the ratio of total chlorophyll *b* [TChl *b*] to [TChl *a*]; (b) the ratio of total chlorophyll *c* [TChl *c*] to [TChl *a*]; (c) the ratio of photosynthetic carotenoids PSC to [TChl *a*]; and (d) the ratio of photoprotective carotenoids PPC to [TChl *a*]. Samples are grouped for different ranges of cell size parameter (S_f) as indicated in the legend. The coefficient of determination was calculated on the basis of all data in the form of a power law (Figures 9b and 9c) and of a linear regression (Figures 9c and 9d).

et al. (2004) suggested that phytoplankton cells adapt to changes in light conditions both by increasing their intracellular pigment content, and by changing the ratio of accessory pigments. They noted that high concentrations of photoprotective pigments are a characteristic feature of surface oligotrophic waters and can also be related to cell size. We observe that an increase in the [PPC]/[TChl *a*] ratio is accompanied by an increase in a_{ph}*(440). About 51% of the variability in a_{ph}*(440) is due to the direct combined effect of the [PPC]/[TChl *a*] ratio and phytoplankton cell size, with the strongest contribution coming from S_f, which explains 46% of the variability (Figures 8d and 9d).

Summarizing the results in Figures 8 and 9, we notice that variations in phytoplankton cell size as well as variations in [PPC]/[TChl *a*] ratio are the main factors responsible for the variability in a_{ph}*(440).

Figure 10 displays variations of SI and [PPC]/[TChl *a*] ratio as a function of [TChl *a*] for diverse areas of the global ocean. As expected, the SI values increase with increasing [TChl *a*] and are within the ranges of SI values found in various regions of the world's ocean, although these measurements were restricted to the surface layer (Bricaud et al., 2004, 2010) (Figure 10a). On average, the phytoplankton community size structure seems to be slightly smaller than those in the Mediterranean Sea and slightly larger than those in the Atlantic Ocean (Figure 10b). As reported in previous studies, the [PPC]/[TChl *a*] ratio decrease according to depth (higher values in surface water) in inverse relation to [TChl *a*] (Bricaud et al., 2004; Organelli et al., 2011). A group of low [PPC]/[TChl *a*] values (>0.2) is also identified in the deeper layer and appears to not be related to [TChl *a*] (Figure 10c) as reported in the Mediterranean Sea by Organelli et al. (2011). As for SI values, the [PPC]/[TChl *a*] values are within the range of those observed in the other areas of the global ocean (Bricaud et al., 2004, 2010). On average, the [PPC]/[TChl *a*] values are slightly higher than those observed in the Mediterranean Sea and in the Atlantic Ocean (Figure 10d). Therefore, the differences in average phytoplankton cell size and [PPC]/[TChl *a*] values can affect the variability in phytoplankton absorption and partially explain

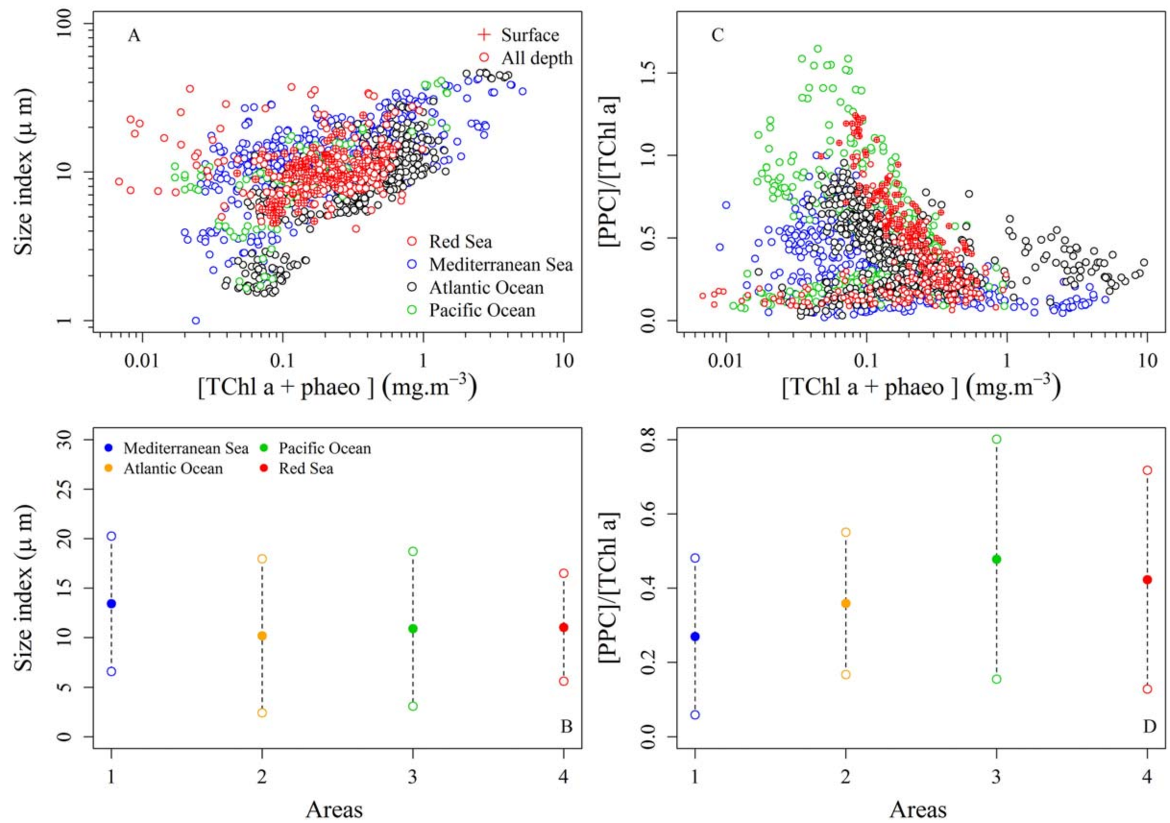

Figure 10. (a) Variations of the size index (SI) estimated from the relative concentrations of some diagnostic pigments (equations (1)–(5)) as a function of [TChl *a*] and (b) average (filled circle) $\pm$ standard deviation (empty circle) SI values; (c) variations of the PPC/[TChl *a*] ratios as a function of [TChl *a*] and (d) average (filled circle) $\pm$ standard deviation (empty circle) PPC/[TChl *a*] values for various areas of the global ocean. Data collected during cruises other than those performed in the Red Sea are taken from Bricaud et al. (2004, 2010).

the higher $a_{ph}(\lambda)$ values at a given [TChl *a*] observed in Red Sea waters compared to other areas of the global ocean. Indeed, our results indicate that phytoplankton cell size associated to changes in PPC pigments are rather well correlated to $a_{ph}^*(\lambda)$. The trend of decreasing cell size is associated to an increase in [PPC]/[TChl *a*] ratio and $a_{ph}^*(\lambda)$ which is consistent with the expectation of higher relative proportions of accessory pigments when the proportion of smaller phytoplankton cells increases (Bricaud et al., 1995; Dupouy et al., 1997; Stuart et al., 1998, 2004). These results reflect the changes in phytoplankton community size structure in response to the environmental conditions encountered in the Red Sea, which is characterized as an oligotrophic region with high light and low nutrient concentrations. *Prochlorococcus* and *Synechococcus* are known to be the most abundant organisms in highly stratified and nutrient depleted oceans between 45°N and 45°S (Al-Najjar et al., 2007; Johnson et al., 2006; Kheireddine et al., 2017; Olson et al., 1990; Partensky et al., 1999; Pearman et al., 2016; Shibl et al., 2014, 2016). They correspond to phytoplankton of small size associated to a high proportion in PPC pigments (mainly zeaxanthin pigment) which is consistent with our observations in this study.

3.4. Influence of Environmental Parameters on $a_{ph}^*(440)$

Recently, Kheireddine et al. (2017) have suggested that latitudinal changes in physicochemical variables, such as temperature and salinity, may influence phytoplankton community size structure in Red Sea waters. Temperature and salinity are known to be important environmental parameters that influence phytoplankton community structure (Ahel et al., 1996; Blanchot et al., 1992; Bouman et al., 2003, 2005; Campbell & Vaulot, 1993; Fehling et al., 2012; Graziano et al., 1996; Hulyal & Kaliwal, 2009; Lohrenz et al., 2003; Loureiro et al., 2006; Moore et al., 1995; Platt et al., 2005; Vaulot & Partensky, 1992; Veldhuis & Kraay, 1993). Thus, the variability around the relationship between $a_{ph}^*(\lambda)$ and [TChl *a*] found in Red Sea waters might also be associated with changes in physicochemical conditions within the basin. In Figure 11, $a_{ph}^*(440)$, temperature

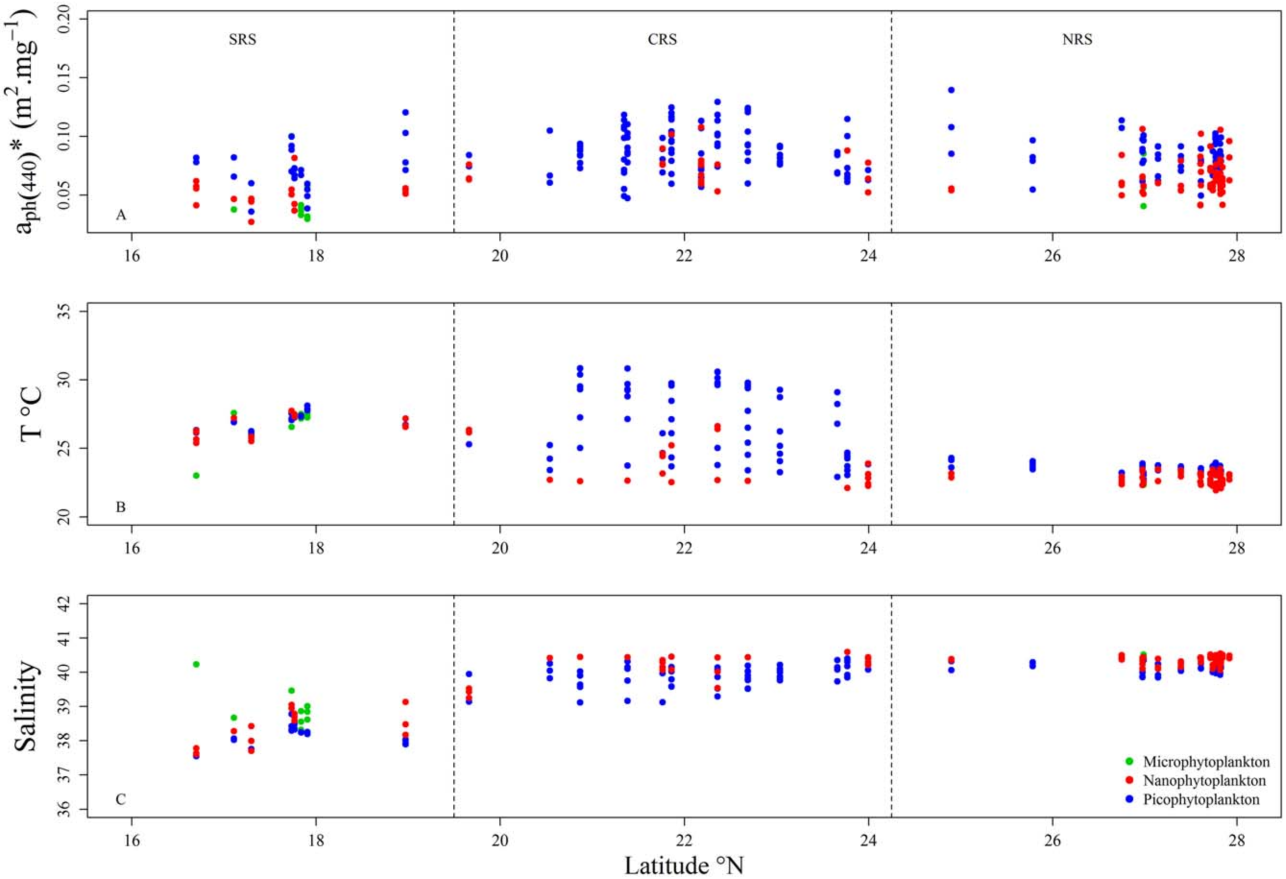

Figure 11. Latitudinal variations of chlorophyll-specific phytoplankton absorption coefficients at (a) 440 nm, $a_{ph}(440)^*$, (b) temperature, and (c) salinity. The delineation of the Northern Red Sea (NRS), the Central Red Sea (CRS), and the Southern Red Sea (SRS) is indicated on each plot. Samples are grouped according to the phytoplankton dominated group (micophytoplankton, nanophytoplankton, or picophytoplankton) as indicated in the legend.

(T °C) and salinity are plotted as a function of the latitude. The spatial distributions of $a_{ph}^*(440)$ and T °C showed similar latitudinal variations (Figures 11a and 11b) although no strong correlation is observed between $a_{ph}^*(440)$ and T °C (not shown). Both parameters tend to increase from the SRS to the CRS and then to decrease from the CRS to the NRS (Figure 11a and 11b). The highest values of $a_{ph}^*(440)$ ($>$0.10 m^2 mg^{-1}) are, generally, consistent with the highest values of T °C ($>$30°C) and high values of salinity (39–40.5) in the CRS which is also the area where the abundance of picophytoplankton (mainly *Prochlorococcus* and *Synechococcus* sp.) is the highest ($>$60% of the total phytoplankton biomass) (Figure 11a–11c). This finding is consistent with observations in the Red Sea (Kheireddine et al., 2017; Shibl et al., 2016) and from other oligotrophic regions (Bouman et al., 2006; Partensky et al., 1999; Zinser et al., 2007) where variations in temperature and salinity influence the distribution of *Prochlorococcus* and *Synechococcus*. The lowest values of $a_{ph}^*(440)$ are found in the two extremities of the basin where the proportions in bigger cells to total phytoplankton biomass are higher than in the rest of the basin, as shown by Kheireddine et al. (2017) based on HPLC measurements collected at the same period or season (Figure 11a).

4. Conclusion

We have shown that the absorption coefficients of phytoplankton and nonalgal particles measured in the Red Sea display a large variability associated with changes in environmental conditions. This variability can affect the proportion of nonalgal particles and the phytoplankton community size structure. The cell size parameter and the proportion in the [PPC]/[TChl *a*] ratio (mainly associated with zeaxanthin pigment) both play a key role in the variability observed in $a_{ph}^*(440)$ (46% and 51%, respectively). Furthermore, values in $a_{ph}(\lambda)$ measured in this study are slightly higher for a given [TChl *a*] value than those estimated from existing global relationships established for oligotrophic waters (Brewin et al., 2011; Bricaud et al., 1995, 2004; Devred et al., 2006), as well as for the Red Sea (Brewin et al., 2015) within the first optical depth and among depths. These higher coefficients are attributed to a higher relative proportion of PPC pigments, and smaller cell size. The $a_{nap}(440)$ coefficients are also higher than those previously observed in oligotrophic waters when [TChl *a*] < 0.1 mg m^{-3} and lower when [TChl *a*] > 0.1 mg m^{-3}. In the clearest waters ([TChl *a*] < 0.1 mg m^{-3}), the contribution of nonalgal particles to total particulate absorption was found to be higher than expected, suggesting the presence of more numerous inorganic (dusts) and/or colored nonalgal particles in these waters. Thus, in situ measurements to quantify and identify these particles in the Red Sea waters including all environmental conditions will be required.

It is known that some existing methods used to retrieve chlorophyll *a* needs to derive $a_p(\lambda)$ from total light absorption and then estimate the chlorophyll *a* based on its relationship with $a_{ph}(\lambda)$ (Garver & Siegel, 1997; Maritorena et al., 2002; Morel et al., 2006; Morel & Maritorena, 2001). This relationship is essential for development of Red Sea algorithms for estimating the diffuse attenuation coefficient of downward irradiance and ocean primary production. Therefore, this study reveals the way to the refinement of ocean color algorithms to more accurately retrieve biogeochemical parameters (chlorophyll *a* concentration, primary production, PFTs, . . .) in Red Sea waters.

Acknowledgments
The authors express their gratitude to the scientists, officers, and crews of the research vessel Thuwal and also the Coastal and Marine Resources Core Lab for logistical support and assistance onboard during the fieldwork. U. Langner is cordially thanked for plotting the map of the Red Sea, L. Solabarrieta and J. Otoadese for their advices and discussions on the results presented here and for reading the manuscript. Alison Chase and the anonymous reviewer are warmly thanked for the constructive comments on a previous version of the manuscript. This study is funded by the King Abdullah University of Science and Technology (KAUST), Kingdom of Saudi Arabia. The data presented in this study are available from the authors upon request (malika.kheireddine@kaust.edu.sa) and are also archived in https://drive.google.com/open?id=0ByAL0hQpcGGPZmItRzh4eXNVdkk.

References

Ahel, M., Barlow, R. G., & Mantoura, R. F. C. (1996). Effect of salinity gradients on the distribution of phytoplankton pigments in a stratified estuary. *Marine Ecology Progress Series*, *143* (1–3), 289–295. https://doi.org/10.3354/meps143289

Allali, K., Bricaud, A., & Claustre, H. (1997). Spatial variations in the chlorophyll-specific absorption coefficients of phytoplankton and photosynthetically active pigments in the equatorial Pacific. *Journal of Geophysical Research*, *102*(C6), 12413–12423. https://doi.org/10.1029/97JC00380

Almahasheer, H., Aljowair, A., Duarte, C. M., & Irigoien, X. (2016). Decadal stability of Red Sea mangroves. *Estuarine Coastal and Shelf Sciences*, *169*, 164–172. https://doi.org/10.1016/j.ecss.2015.11.027

Al-Najjar, T., Badran, M. I., Richter, C., Meyerhoefer, M., & Sommer, U. (2007). Seasonal dynamics of phytoplankton in the Gulf of Aqaba, Red Sea. *Hydrobiologia*, *579*, 69–83. https://doi.org/10.1007/s10750-006-0365-z

Al-Taani, A. A., Rashdan, M., & Khashashneh, S. (2015). Atmospheric dry deposition of mineral dust to the Gulf of Aqaba, Red Sea: Rate and trace elements. *Marine Pollution Bulletin*, *92* (1–2), 252–258. https://doi.org/10.1016/j.marpolbul.2014.11.047

Atlas, D., & Bannister, T. T. (1980). Dependence of mean spectral extinction coefficient of phytoplankton on depth, water color, and species. *Limnology and Oceanography*, *25*(1), 157–159. https://doi.org/10.4319/lo.1980.25.1.0157

Barlow, R., Kyewalyanga, M., Sessions, H., Van Den Berg, M., & Morris, T. (2008). Phytoplankton pigments, functional types, and absorption properties in the Delagoa and Natal Bights of the Agulhas ecosystem. *Estuarine Coastal and Shelf Sciences*, *80*(2), 201–211.

Barlow, R. G., Aiken, J., Moore, G. F., Holligan, P. M., & Lavender, S. (2004). Pigment adaptations in surface phytoplankton along the eastern boundary of the Atlantic Ocean. *Marine Ecology Progress Series*, *281*, 13–26. https://doi.org/10.3354/meps281013

Belkin, I. M. (2009). Rapid warming of large marine ecosystems. *Progress in Oceanography*, *81*(1–4), 207–213. https://doi.org/10.1016/j.pocean.2009.04.011

Berumen, M. L., Hoey, A., Bass, W., Bouwmeester, J., Catania, D., Cochran, J. E., et al. (2013). The status of coral reef ecology research in the Red Sea. *Coral Reefs*, *32*(3), 737–748. https://doi.org/10.1007/s00338-013-1055-8

Blanchot, J., Rodier, M., & Lebouteiller, A. (1992). Effect of El-Niño southern oscillation events on the distribution and abundance of phytoplankton in the Western Pacific Tropical Ocean along 165°E. *Journal of Plankton Research*, *14*(1), 137–156. https://doi.org/10.1093/plankt/14.1.137

Boss, E., Gildor, H., Slade, W., Sokoletsky, L., Oren, A., & Loftin, J. (2013a). Optical properties of the Dead Sea. *Journal of Geophysical Research: Oceans*, *118*, 1821–1829. https://doi.org/10.1002/jgrc.20109

Boss, E., Picheral, M., Leeuw, T., Chase, A., Karsenti, E., Gorsky, G., et al. (2013b). The characteristics of particulate absorption, scattering and attenuation coefficients in the surface ocean; contribution of the Tara Oceans expedition. *Method Oceanography*, *7*, 52–62. https://doi.org/10.1016/j.mio.201311.002

Boss, E. S., Collier, R., Larson, G., Fennel, K., & Pegau, S. W. (2007). Measurements of spectral optical properties and their relation to biogeochemical variables and processes in Crater Lake, Crater Lake National Park, OR. *Hydrobiologica*, *574*, 149–159. https://doi.org/10.1007/s10750-006-2609-3

Bouman, H. A., Platt, T., Sathyendranath, S., Li, W. K. W., Stuart, V., Fuentes-Yaco, C., et al. (2003). Temperature as indicator of optical properties and community structure of marine phytoplankton: Implications for remote sensing. *Marine Ecology Progress Series*, *258*, 19–30. https://doi.org/10.3354/meps258019

Bouman, H. A., Platt, T., Sathyendranath, S., & Stuart, V. (2005). Dependence of light-saturated photosynthesis on temperature and community structure. *Deep Sea Research Part I: Oceanographic Research Papers*, *52*(7), 1284–1299. https://doi.org/10.1016/j.dsr.2005.01.008

Bouman, H. A., Ulloa, O., Canlan, D. J., Zwirglmaier, K., Li, W. K. W., Platt, T., et al. (2006). Oceanographic basis of the global surface distribution of *Prochlorococcus* ecotypes. *Science*, *312*(5775), 918–921. https://doi.org/10.1126/science.1122692

Bracher, A., Bouman, H. A., Brewin, R. J. W., Bricaud, A., Brotas, V., Ciotti, A. M., et al. (2017). Obtaining phytoplankton diversity from ocean color: A scientific roadmap for future development. *Frontiers in Marine Sciences*, *4*, 55. https://doi.org/10.3389/fmars.2017.00055

Brewin, R. J. W., Dall'Olmo, G., Sathyendranath, S., & Hardman-Mountford, N. J. (2012). Particle backscattering as a function of chlorophyll and phytoplankton size structure in the open-ocean. *Optics Express*, *20*, 17632–17652. https://doi.org/10.1364/OE.20.017632

Brewin, R. J. W., Devred, E., Sathyendranath, S., Lavender, S. J., & Hardman-Mountford, N. J. (2011). Model of phytoplankton absorption based on three size classes. *Applied Optics*, *50*(22), 4535–4549. https://doi.org/10.1364/AO.50.004535

Brewin, R. J. W., Raitsos, D. E., Dall'Olmo, G., Zarokanellos, N., Jackson, T., Racault, M.-F., et al. (2015). Regional ocean-colour chlorophyll algorithms for the Red Sea. *Remote Sensing Environment*, *165*, 64–85. https://doi.org/10.1016/j.rse.2015.04.024

Bricaud, A., Babin, M., Claustre, H., Ras, J., & Tieche, F. (2010). Light absorption properties and absorption budget of Southeast Pacific waters. *Journal of Geophysical Research*, *115*, C08009. https://doi.org/10.1029/2009JC005517

Bricaud, A., Babin, M., Morel, A., & Claustre, H. (1995). Variability in the chlorophyll-specific absorption coefficients of natural phytoplankton: Analysis and parameterization. *Journal of Geophysical Research*, *100*(C7), 13321–13332. https://doi.org/10.1029/95JC00463

Bricaud, A., Claustre, H., Ras, J., & Oubelkheir, K. (2004). Natural variability of phytoplanktonic absorption in oceanic waters: Influence of the size structure of algal populations. *Journal of Geophysical Research*, *109*, C11010. https://doi.org/10.1029/2004JC002419

Bricaud, A., & Morel, A. (1986). Light attenuation and scattering by phytoplanktonic cells: A theoretical modeling. *Applied Optics*, *25*(4), 571–580.

Bricaud, A., Morel, A., Babin, M., Allali, K., & Claustre, H. (1998). Variations of light absorption by suspended particles with chlorophyll *a* concentration in oceanic (case 1) waters: Analysis and implications for bio-optical models. *Journal of Geophysical Research*, *103*(C13), 31033–31044. https://doi.org/10.1029/98JC02712

Bricaud, A., & Stramski, D. (1990). Spectral absorption coefficients of living phytoplankton and nonalgal biogenous matter: A comparison between the Peru upwelling area and the Sargasso Sea. *Limnology and Oceanography*, *35*(3), 562–582. https://doi.org/10.4319/lo.1990.35.3.0562

Brunelle, C. B., Larouche, P., & Gosselin, M. (2012). Variability of phytoplankton light absorption in Canadian Arctic seas. *Journal of Geophysical Research*, *117*, C00G17. https://doi.org/10.1029/2011JC007345

Buesseler, K. O., Lamborg, C. H., Boyd, P. W., Lam, P. J., Trull, T. W., Bidigare, R. R., et al. (2007). Revisiting Carbon flux through the ocean's twilight zone. *Science*, *316*, 567–570.

Campbell, L., & Vaulot, D. (1993). Photosynthetic picoplankton community structure in the subtropical North Pacific Ocean near Hawaii (station ALOHA). *Deep Sea Research Part I: Oceanographic Research Papers*, *40*(10), 2043–2060. https://doi.org/10.1016/0967-0637(93)90044-4

Churchill, J. H., Bower, A. S., McCorkle, D. C., & Abualnaja, Y. (2014). The transport of nutrient-rich Indian Ocean water through the Red Sea and into coastal reef systems. *Journal of Marine Research*, *72*(3), 165–181. https://doi.org/10.1357/002224014814901994

Ciotti, A. M., & Bricaud, A. (2006). Retrievals of a size parameter for phytoplankton and spectral light absorption by colored detrital matter from water-leaving radiances at SeaWiFS channels in a continental shelf region off Brazil. *Limnology and Oceanography Methods*, *4*, 237–253. https://doi.org/10.4319/lom.2006.4.237

Ciotti, A. M., Cullen, J. J., & Lewis, M. R. (1999). A semi-analytical model of the influence of phytoplankton community structure on the relationship between light attenuation and ocean color. *Journal of Geophysical Research*, *104*(C1), 1559–1578. https://doi.org/10.1029/1998JC900021

Ciotti, A. M., Lewis, M. R., & Cullen, J. J. (2002). Assessment of the relationships between dominant cell size in natural phytoplankton communities and the spectral shape of the absorption coefficient. *Limnology and Oceanography*, *47*(2), 404–417. https://doi.org/10.4319/lo.2002.47.2.0404

Cleveland, J. S. (1995). Regional models for phytoplankton absorption as a function of chlorophyll *a* concentration. *Journal of Geophysical Research*, *100*(C7), 13333–13344. https://doi.org/10.1029/95JC00532

Dall'Olmo, G., Boss, E., Behrenfeld, M. J., & Westberry, T. K. (2012). Particulate optical scattering coefficients along an Atlantic Meridional Transect. *Optics Express*, *20*(19), 21532–21551. https://doi.org/10.1364/OE.20.021532

Dall'Olmo, G., Westberry, T. K., Behrenfeld, M. J., Boss, E., & Slade, W. H. (2009). Significant contribution of large particles to optical backscattering in the open ocean. *Biogeosciences*, *6*(6), 947–967. https://doi.org/10.5194/bg-6-947-2009

Devred, E., Sathyendranath, S., Stuart, V., Maass, H., Ulloa, O., & Platt, T. (2006). A two-component model of phytoplankton absorption in the open ocean: Theory and applications. *Journal of Geophysical Research*, *111*, C03011. https://doi.org/10.1029/2005JC002880

Dreano, D., Raitsos, D. E., Gittings, J., Krokos, G., & Hoteit, I. (2016). The Gulf of Aden intermediate water intrusion regulates the Southern Red Sea summer phytoplankton blooms. *PLoS ONE*, *11*(12), e0168440. https://doi.org/10.1371/journal.pone.0168440

Dupouy, C., Neveux, J., & Andre, J. M. (1997). Spectral absorption coefficient of photosynthetically active pigments in the equatorial Pacific Ocean (165°E–150°W). *Deep Sea Research Part II: Topical Studies in Oceanography*, *44*(9–10), 1881–1906. https://doi.org/10.1016/S0967-0645(97)00078-7

Eppley, R. W., Holmes, R. W., & Strickland, J. D., II (1967). Sinking rates of marine phytoplankton measured with a fluorometer. *Journal of Experimental Marine Biology and Ecology*, *1*, 191–208. https://doi.org/10.1016/0022-0981(67)90014-7

Fehling, J., Davidson, K., Bolch, C. J. S., Brand, T. D., & Narayanaswamy, B. E. (2012). The relationship between phytoplankton distribution and water column characteristics in North West European Shelf Sea Waters. *PLoS ONE*, *7*(3), e34098. https://doi.org/10.1371/journal.pone.0034098

Ferreira, A., Stramski, D., Garcia, C. A. E., Garcia, V. M. T., Ciotti, A. M., & Mendes, C. R. B. (2013). Variability in light absorption and scattering of phytoplankton in Patagonian waters: Role of community size structure and pigment composition. *Journal of Geophysical Research: Oceans*, *118*, 698–714. https://doi.org/10.1002/jgrc.20082

Garver, S. A., & Siegel, D. A. (1997). Inherent optical property inversion of ocean color spectra and its biogeochemical interpretation: 1. Time series from the Sargasso Sea. *Journal of Geophysical Research*, *102*(C8), 18607–18625. https://doi.org/10.1029/96JC03243

Ginoux, P., Prospero, J. M., Gill, T. E., Hsu, N. C., & Zhao, M. (2012). Global-scale attribution of anthropogenic and natural dust sources and their emission rates based on MODIS Deep Blue aerosol products. *Reviews of Geophysics*, *50*, RG3005. https://doi.org/10.1029/2012RG000388

Gittings, J. A., Raitsos, D. E., Racault, M.-F., Brewin, R. J., Pradhan, Y., Sathyendranath, S., et al. (2017). Seasonal phytoplankton blooms in the Gulf of Aden revealed by remote sensing. *Remote Sensing Environment*, *189*(2017), 56–66. https://doi.org/10.1016/j.rse.2016.10.043

Gordon, H. R., & McCluney, W. R. (1975). Estimation of the depth of sunlight penetration in the sea for remote sensing. *Applied Optics*, *14*(2), 413–416. https://doi.org/10.1364/AO.14.000413

Graziano, L. M., Geider, R. J., Li, W. K. W., & Olaizola, M. (1996). Nitrogen limitation of North Atlantic phytoplankton: Analysis of physiological condition in nutrient enrichment experiments. *Aquatic Microbial Ecology*, *11*(1), 53–64. https://doi.org/10.3354/ame011053

Hulyal, S. B., & Kaliwal, B. B. (2009). Dynamics of phytoplankton in relation to physico-chemical factors of Almatti reservoir of Bijapur District, Karnataka State. *Environmental Monitoring and Assessment*, *153*(1–4), 45–59. https://doi.org/10.1007/s10661-008-0335-1

Ismael, A. A. (2015). Phytoplankton of the Red Sea. In *The Red Sea* (pp. 567–583). Berlin, Germany: Springer.

Johnson, Z. I., Zinser, E. R., Coe, A., McNulty, N. P., Woodward, E. M. S., & Chisholm, S. W. (2006). Niche partitioning among *Prochlorococcus* ecotypes along ocean-scale environmental gradients. *Science*, *311*(5768), 1737–1740. https://doi.org/10.1126/science.1118052

Kheireddine, M., Ouhssain, M., Claustre, H., Uitz, J., Gentili, B., & Jones, B. H. (2017). Assessing pigment-based phytoplankton community distributions in the Red Sea. *Frontiers in Marine Science*, *4*, 2296–7745. https://doi.org/10.3389/fmars.2017.00132

Kiefer, D. A., & Mitchell, B. G. (1983). A simple, steady-state description of phytoplankton growth based on absorption cross-section and quantum efficiency. *Limnology and Oceanography*, *28*(4), 770–776. https://doi.org/10.4319/lo.1983.28.4.0770

Kirk, J. T. (1994). *Light and photosynthesis in aquatic ecosystems* (401 pp.). Cambridge, UK: Cambridge University Press.

Kishino, M., Takahashi, M., Okami, N., & Ichimura, S. (1985). Estimation of the spectral absorption coefficients of phytoplankton in the sea. *Bulletin of Marine Science*, *37*(2), 634–642.

Lekunberri, I., Lefort, T., Romero, E., Vazquez-Dominguez, E., Romera-Castillo, C., Marrase, C., et al. (2010). Effects of a dust deposition event on coastal marine microbial abundance and activity, bacterial community structure and ecosystem function. *Journal of Plankton Research*, *32*(4), 381–396. https://doi.org/10.1093/plankt/fbp137

Le Quéré, C., Harrison, S. P., Prentice, I. C., Buitenhuis, E. T., Aumont, O., Bopp, L., et al. (2005). Ecosystem dynamics based on plankton functional types for global ocean biogeochemistry models. *Global Change Biology*, *11*(11), 2016–2040. https://doi.org/10.1111/j.1365-2468.2005.01004.x

Lohrenz, S. E., Weidemann, A. D., & Tuel, M. (2003). Phytoplankton spectral absorption as influenced by community size structure and pigment composition. *Journal of Plankton Research*, *25*(1), 35–61. https://doi.org/10.1093/plankt/25.1.35

Longhurst, A. (2007). Toward an ecological geography of the sea. In *Ecological geography of the sea* (pp. 1–17). Amsterdam, the Netherlands: Elsevier.

Loureiro, S., Newton, A., & Icely, J. (2006). Boundary conditions for the European water framework directive in the ria Formosa lagoon, Portugal (physico-chemical and phytoplankton quality elements). *Estuarine, Coastal and Shelf Science*, *67*(3), 382–398. https://doi.org/10.1016/j.ecss.2005.11.029

Lutz, V. A., Sathyendranath, S., & Head, E. J. H. (1996). Absorption coefficient of phytoplankton: Regional variations in the North Atlantic. *Marine Ecology Progress Series*, *135*(1–3), 197–213. https://doi.org/10.3354/meps135197

Majchrowski, R., & Ostrowska, M. (2000). Influence of photo- and chromatic acclimation on pigment composition in the sea. *Oceanologia*, *42*(2), 157–175. https://doi.org/10.1029/2002JD002536

Maritorena, S., Siegel, D. A., & Peterson, A. R. (2002). Optimization of a semianalytical ocean color model for global-scale applications. *Applied Optics*, *41*(15), 2705–2714. https://doi.org/10.1364/AO.41.002705

McCave, I. N. (1975). Vertical flux of particles in the ocean. *Deep Sea Research and Oceanographic Abstracts*, *22*(7), 491–502.

Mitchell, B. G., Kahru, M., Wieland, J., & Stramska, M. (2003). Determination of spectral absorption coefficients of particles, dissolved material and phytoplankton for discrete water samples. In J. L. Mueller, G. S. Fargion, & C. R. McClain (Eds.), *Ocean optics protocols for satellite ocean color sensor validation, revision 4, volume IV: Inherent optical properties: Instruments, characterizations, field measurements and data analysis protocols*. Greenbelt, MD: NASA.

Mitchell, B. G., & Kiefer, D. A. (1988). Variability in pigment specific particulate fluorescence and absorption spectra in the northeastern Pacific Ocean. *Deep Sea Research Part A. Oceanographic Research Papers*, *35*(5), 665–689.

Moore, L. R., Goericke, R., & Chisholm, S. W. (1995). Comparative physiology of *Synechococcus* and *Prochlorococcus*: Influence of light and temperature on growth, pigments, fluorescence and absorptive properties. *Marine Ecology Progress Series*, *116*(1–3), 259–275.

Morales-Baquero, R., Pulido-Villena, E., & Reche, I. (2013). Chemical signature of Saharan dust on dry and wet atmospheric deposition in the south-western Mediterranean region. *Tellus, Series B*, *65*, 18720. https://doi.org/10.3402/tellusb.v65i0.18720

Morel, A. (1988). Optical modeling of the upper ocean in relation to its biogenous matter content (case I waters). *Journal of Geophysical Research*, *93*(C9), 10749–10768. http://dx.doi.org/10.1029/JC093iC09p10749

Morel, A. (1991). Light and marine photosynthesis: A spectral model with geochemical and climatological implications. *Progress in Oceanography*, *26*(3), 263–306. https://doi.org/10.1016/0079-6611(91)90004-6

Morel, A., & Bricaud, A. (1981). Theoretical results concerning light absorption in a discrete medium, and application to specific absorption of phytoplankton. *Deep Sea Research Part A. Oceanographic Research Papers*, *28*(11), 1375–1393.

Morel, A., Gentili, B., Chami, M., & Ras, J. (2006). Bio-optical properties of high chlorophyll Case 1 waters and of yellow-substance-dominated Case 2 waters. *Deep Sea Research Part I: Oceanographic Research Papers*, *53*(9), 1439–1459. https://doi.org/10.1016/j.dsr.2006.07.007

Morel, A., Huot, Y., Gentili, B., Werdell, P. J., Hooker, S. B., & Franz, B. A. (2007). Examining the consistency of products derived from various ocean color sensors in open ocean (Case 1) waters in the perspective of a multi-sensor approach. *Remote Sensing Environment*, *111*(1), 69–88. https://doi.org/10.1016/j.rse.2007.03.012

Morel, A., & Maritorena, S. (2001). Bio-optical properties of oceanic waters: A reappraisal. *Journal of Geophysical Research*, *106*(C4), 7163–7180. https://doi.org/10.1029/2000JC000319

Neumann, A. C., & McGill, D. A. (1962). Circulation of the Red Sea in early summer. *Deep Sea Research and Oceanographic Abstracts*, *8*(3/4), 223–235.

Olson, R. J., Chisholm, S. W., Zettler, E. R., & Armbrust, E. V. (1990). Pigments, size, and distribution of *Synechococcus* in the North Atlantic and Pacific Oceans. *Limnology and Oceanography*, *35*(1), 45–58. https://doi.org/10.4319/lo.1990.35.1.0045

Organelli, E., Bricaud, A., Antoine, D., & Matsuoka, A. (2014). Seasonal dynamics of light absorption by chromophoric dissolved organic matter (CDOM) in the NW Mediterranean Sea (BOUSSOLE site). *Deep Sea Research Part I: Oceanographic Research Papers*, *91*, 72–85. https://doi.org/10.1016/j.dsr.2014.05.003

Organelli, E., Bricaud, A., Antoine, D., & Uitz, J. (2013). Multivariate approach for the retrieval of phytoplankton size structure from measured light absorption spectra in the Mediterranean Sea (BOUSSOLE site). *Applied Optics*, *52*(11), 2257–2273. https://doi.org/10.1364/AO.52.002257

Organelli, E., Claustre, H., Bricaud, A., Barbieux, M., Uitz, J., D'Ortenzio, F., et al. (2017). Bio-optical anomalies in the world's oceans: An investigation on the diffuse attenuation coefficients for downward irradiance derived from Biogeochemical Argo float measurements. *Journal of Geophysical Research: Oceans*, *122*, 3543–3564. https://doi.org/10.1002/2016JC012629

Organelli, E., Nuccio, C., Melillo, C., & Massi, L. (2011). Relationships between phytoplankton light absorption, pigment composition and size structure in offshore areas of the Mediterranean Sea. *Advances in Oceanography and Limnology*, *2*(2), 107–123. https://doi.org/10.1080/19475721.2011.607489

Partensky, F., Hess, W. R., & Vaulot, D. (1999). *Prochlorococcus*, a marine photosynthetic prokaryote of global significance. *Microbiology and Molecular Biology Reviews*, *63*(1), 106.

Patzert, W. C. (1974). Wind-induced reversal in Red Sea circulation. *Deep Sea Research and Oceanographic Abstracts*, *21*(2), 109–121.

Pearman, J. K., Kurten, S., Sarma, Y. V. B., Jones, B. H., & Carvalho, S. (2016). Biodiversity patterns of plankton assemblages at the extremes of the Red Sea. *FEMS Microbiology Ecology*, *92*(3), fiw002. https://doi.org/10.1093/femsec/fiw002

Perez, G., Queimalinos, C., Balseiro, E., & Modenutti, B. (2007). Phytoplankton absorption spectra along the water column in deep North Patagonian Andean lakes (Argentina). *Limnologica*, *37*(1), 3–16. https://doi.org/10.1016/j.limno.2006.08.005

Platt, T., Bouman, H., Devred, E., Fuentes-Yaco, C., & Sathyendranath, S. (2005). Physical forcing and phytoplankton distributions. *Scientia Marina*, *69*, 55–73.

Platt, T., & Sathyendranath, S. (1988). Oceanic primary production: Estimation by remote sensing at local and regional scales. *Science*, *241*(4873), 1613–1620. https://doi.org/10.1126/science.241.4873.1613

Ploug, H., Iversen, M. H., & Fisher, G. (2008). Ballast sinking velocity, and apparent diffusivity within marine snow and zooplankton fecal pellets: Implications for substrate turnover by attached bacteria. *Limnology and Oceanography*, *53*, 1878–1886.

Prakash, P. J., Stenchikov, G., Kalenderski, S., Osipov, S., & Bangalath, H. (2015). The impact of dust storms on the Arabian Peninsula and the Red Sea. *Atmospheric Chemistry and Physics*, *15*(1), 199–222. https://doi.org/10.5194/acp-15-199-2015

Prospero, J. M., Ginoux, P., Torres, O., Nicholson, S. E., & Gill, T. E. (2002). Environmental characterization of global sources of atmospheric soil dust identified with the Nimbus 7 Total Ozone Mapping Spectrometer (TOMS) absorbing aerosol product. *Reviews Geophysics*, *40*(1), 1002. https://doi.org/10.1029/2000RG000095

Racault, M.-F., Raitsos, D. E., Berumen, M. L., Brewin, R. J. W., Platt, T., Sathyendranath, S., et al. (2015). Phytoplankton phenology indices in coral reef ecosystems: Application to ocean-color observations in the Red Sea. *Remote Sensing Environment*, *160*, 222–234. https://doi.org/10.1016/j.rse.2015.01.019

Raitsos, D. E., Hoteit, I., Prihartato, P. K., Chronis, T., Triantafyllou, G., & Abualnaja, Y. (2011). Abrupt warming of the Red Sea. *Geophysical Research Letters*, *38*, L14601. https://doi.org/10.1029/2011GL047984

Raitsos, D. E., Pradhan, Y., Brewin, R. J. W., Stenchikov, G., & Hoteit, I. (2013). Remote sensing the phytoplankton seasonal succession of the Red Sea. *PLoS ONE*, *8*(6), e64909. https://doi.org/10.1371/journal.pone.0064909

Raitsos, D. E., Yi, X., Platt, T., Racault, M.-F., Brewin, R. J. W., Pradhan, Y., et al. (2015). Monsoon oscillations regulate fertility of the Red Sea. *Geophysical Research Letters*, *42*, 855–862. https://doi.org/10.1002/2014GL062882

Ras, J., Claustre, H., & Uitz, J. (2008). Spatial variability of phytoplankton pigment distributions in the Subtropical South Pacific Ocean: Comparison between in situ and predicted data. *Biogeosciences*, *5*(2), 353–369. https://doi.org/10.5194/bg-5-353-2008

Reche, I., Ortega-Retuerta, E., Romera, O., Pulido-Villena, E., Morales-Baquero, R., & Casamayor, E. O. (2009). Effect of Saharan dust inputs on bacterial activity and community composition in Mediterranean lakes and reservoirs. *Limnology and Oceanography*, *54*(3), 869–879. https://doi.org/10.4319/lo.2009.54.3.0869

Roesler, C. S., & Barnard, A. H. (2013). Optical proxy for phytoplankton biomass in the absence of photophysiology: Rethinking the absorption line height. *Methods in Oceanography*, *7*, 79–94. https://doi.org/10.1016/j.mio.2013.12.003

Roesler, C. S., & Perry, M. J. (1995). In situ phytoplankton absorption, fluorescence emission, and particulate backscattering spectra determined from reflectance. *Journal of Geophysical Research*, *100*(C7), 13279–13294. https://doi.org/10.1029/95JC00455

Roy, S., Sathyendranath, S., & Platt, T. (2011). Retrieval of phytoplankton size from bio-optical measurements: Theory and applications. *Journal of the Royal Society Interface*, *8*(58), 650–660. https://doi.org/10.1098/rsif.2010.0503

Sathyendranath, S., Cota, G., Stuart, V., Maass, H., & Platt, T. (2001). Remote sensing of phytoplankton pigments: A comparison of empirical and theoretical approaches. *International Journal of Remote Sensing*, *22*(2–3), 249–273. https://doi.org/10.1080/014311601449925

Sathyendranath, S., & Platt, T. (1988). The spectral irradiance field at the surface and in the interior of the ocean: A model for applications in oceanography and remote sensing. *Journal of Geophysical Research*, *93*(C8), 9270–9280. https://doi.org/10.1029/JC093iC08p09270

Sathyendranath, S., Platt, T., Stuart, V., Irwin, B. D., Veldhuis, M. J. W., Kraay, G. W., et al. (1996). Some bio-optical characteristics of phytoplankton in the NW Indian Ocean. *Marine Ecology Progress Series*, *132*(1–3), 299–311.

Sathyendranath, S., Stuart, V., Irwin, B. D., Maass, H., Savidge, G., Gilpin, L., et al. (1999). Seasonal variations in bio-optical properties of phytoplankton in the Arabian Sea. *Deep Sea Research Part II: Topical Studies in Oceanography*, *46* (3–4), 633–653. https://doi.org/10.1016/S0967-0645(98)00121-0

Sathyendranath, S., Stuart, V., Platt, T., Bouman, H., Ulloa, O., & Maass, H. (2005). Remote sensing of ocean colour: Towards algorithms for retrieval of pigment composition. *Indian Journal of Marine Sciences*, *34*(4), 333–340.

Sawall, Y., Al-Sofyani, A., Banguera-Hinestroza, E., & Voolstra, C. R. (2014). Spatio-temporal analyses of Symbiodinium physiology of the coral Pocillopora verrucosa along large-scale nutrient and temperature gradients in the Red Sea. *PLos ONE*, *9*(8), e103179.

Shibl, A. A., Haroon, M. F., Ngugi, D. K., Thompson, L. R., & Stingl, U. (2016). Distribution of *Prochlorococcus* ecotypes in the Red Sea basin based on analyses of rpoC1 sequences. *Frontiers in Marine Science*, *3*, 104. https://doi.org/10.3389/fmars.2016.00104

Shibl, A. A., Thompson, L. R., Ngugi, D. K., & Stingl, U. (2014). Distribution and diversity of *Prochlorococcus* ecotypes in the Red Sea. *FEMS Microbiology Letters*, *356*(1), 118–126. https://doi.org/10.1111/1574-6968.12490

Sofianos, S. S., & Johns, W. E. (2003). An Oceanic General Circulation Model (OGCM) investigation of the Red Sea circulation: 2. Three-dimensional circulation in the Red Sea. *Journal of Geophysical Research*, *108*(C3), 2002. https://doi.org/10.1029/2001JC001184

Sofianos, S. S., & Johns, W. E. (2007). Observations of the summer red sea circulation. *Journal of Geophysical Research*, *112*, C06025. https://doi.org/10.1029/2006JC003886

Stemmann, L., Jackson, G. A., & Ianson, D. (2004). A vertical model of particle size distributions and fluxes in the midwater column that includes biological and physical processes—Part I: Model formulation. *Deep Sea Research Part I: Oceanographic Research Papers*, *51*(7), 865–884. https://doi.org/10.1016/j.dsr.2004.03.001

Stramski, D., Reynolds, R. A., Kaczmarek, S., Uitz, J., & Zheng, G. M. (2015). Correction of pathlength amplification in the filter-pad technique for measurements of particulate absorption coefficient in the visible spectral region. *Applied Optics*, *54*(22), 6763–6782. https://doi.org/10.1364/AO.54.006763

Stuart, V., Sathyendranath, S., Platt, T., Maass, H., & Irwin, B. D. (1998). Pigments and species composition of natural phytoplankton populations: Effect on the absorption spectra. *Journal of Plankton Research*, *20*(2), 187–217. https://doi.org/10.1093/plankt/20.2.187

Stuart, V., Ulloa, O., Alarcon, G., Sathyendranath, S., Major, H., Head, E. J. H., et al. (2004). Bio-optical characteristics of phytoplankton populations in the upwelling system off the coast of Chile. *Revista Chilena De Historia Natural*, *77*(1), 87–105. https://doi.org/10.4067/S0716-078X2004000100008

Suzuki, K., Kishino, M., Sasaoka, K., Saitoh, S., & Saino, T. (1998). Chlorophyll-specific absorption coefficients and pigments of phytoplankton off Sanriku, northwestern North Pacific. *Journal of Oceanography*, *54*, 517–526. https://doi.org/10.1007/BF02742453

Tilstone, G. H., Miller, P. I., Brewin, R. J. W., & Priede, I. G. (2014). Enhancement of primary production in the North Atlantic outside of the spring bloom, identified by remote sensing of ocean colour and temperature. *Remote Sensing Environment*, *146*, 77–86. https://doi.org/10.1016/j.rse.2013.04.021

Triantafyllou, G., Yao, F., Petihakis, G., Tsiaras, K. P., Raitsos, D. E., & Hoteit, I. (2014). Exploring the Red Sea seasonal ecosystem functioning using a three-dimensional biophysical model. *Journal of Geophysical Research: Oceans*, *119*, 1791–1811. https://doi.org/10.1002/2013JC009641

Uitz, J., Claustre, H., Gentili, B., & Stramski, D. (2010). Phytoplankton class-specific primary production in the world's oceans: Seasonal and interannual variability from satellite observations. *Global Biogeochemical Cycles*, *24*, GB3016. https://doi.org/10.1029/2009GB003680

Uitz, J., Claustre, H., Morel, A., & Hooker, S. B. (2006). Vertical distribution of phytoplankton communities in open ocean: An assessment based on surface chlorophyll. *Journal of Geophysical Research*, *111*, C08005. https://doi.org/10.1029/2005JC003207

Uitz, J., Huot, Y., Bruyant, F., Babin, M., & Claustre, H. (2008). Relating phytoplankton photophysiological properties to community structure on large scales. *Limnology and Oceanography*, *53*(2), 614–630. https://doi.org/10.2307/40006445

Uitz, J., Stramski, D., Reynolds, R. A., & Dubranna, J. (2015). Assessing phytoplankton community composition from hyperspectral measurements of phytoplankton absorption coefficient and remote-sensing reflectance in open-ocean environments. *Remote Sensing Environment*, *171*, 58–74. https://doi.org/10.1016/j.rse.2015.09.027

Vaulot, D., & Partensky, E. (1992). Cell cycle of prochlorophytes in the north western Mediterranean Sea. *Deep Sea Research Part A. Oceanographic Research Papers*, *39*(5A), 727–742. https://doi.org/10.1016/0198-0149(92)90117-C

Veldhuis, M. J. W., & Kraay, G. W. (1993). Cell abundance and fluorescence of picoplankton in relation to growth irradiance and nitrogen availability in the Red Sea. *Netherlands Journal of Sea Research*, *31*(2), 135–145. https://doi.org/10.1016/0077-7579(93)90003-B

Vidussi, F., Claustre, H., Manca, B. B., Luchetta, A., & Marty, J. C. (2001). Phytoplankton pigment distribution in relation to upper thermocline circulation in the eastern Mediterranean Sea during winter. *Journal of Geophysical Research*, *106*(C9), 19939–19956. https://doi.org/10.1029/1999JC000308

Vijayan, A. K., & Somayajula, S. A. (2014). Effect of accessory pigment composition on the absorption characteristics of a dinoflagellate bloom in a coastal embayment. *Oceanologia*, *56*(1), 107–124. https://doi.org/10.5697/oc.56-1.107

Wafar, M., Ashraf, M., Manikandan, K. P., Qurban, M. A., & Kattan, Y. (2016). Propagation of Gulf of Aden Intermediate Water (GAIW) in the Red Sea during autumn and its importance to biological production. *Journal of Marine Systems*, *154*, 243–251. https://doi.org/10.1016/j.jmarsys.2015.10.016

Wang, S. Q., Ishizaka, J., Hirawake, T., Watanabe, Y., Zhu, Y. L., Hayashi, M., et al. (2015). Remote estimation of phytoplankton size fractions using the spectral shape of light absorption. *Optics Express*, *23*(8), 10301–10318. https://doi.org/10.1364/OE.23.010301

Westberry, T. K., Dall'Olmo, G., Boss, E., Behrenfeld, M. J., & Moutin, T. (2010). Coherence of particulate beam attenuation and backscattering coefficients in diverse open ocean environments. *Optics Express*, *18*(15), 15419–15425. https://doi.org/10.1364/OE.18.015419

Zinser, E. R., Johnson, Z. I., Coe, A., Karaca, E., Veneziano, D., & Chisholm, S. W. (2007). Influence of light and temperature on *Prochlorococcus* ecotype distributions in the Atlantic Ocean. *Limnology Oceanography*, *52*(5), 2205–2220. https://doi.org/10.4319/lo.2007.52.5.2205